Hannelore Olsen

A CFD Study on How Fish Affect the Flow Inside Closed Fish Farming Cages

Master's Thesis

Trondheim, June 5, 2019

TMR4930 – Marine Technology, Master's Thesis

Norwegian University of Science and Technology
Faculty of Engineering Science
Department of Marine Technology

NTNU

*This thesis is dedicated to Mother Nature, the environment,
in hope of a sustainable future.*

Preface

A CFD Study on How Fish Affect the Flow Inside Closed Fish Farming Cages was written for TMR4930 – Marine Technology, Master's Thesis, during the spring semester 2019. It is the final requirement in fulfilling the Masters' Degree Program ICT & Marine Technology at Norwegian University of Science and Technology (NTNU). The aim is to obtain and provide new knowledge through a scientific research period of twenty weeks, counting for 30 study points. This thesis builds upon the review and preparation study done during the specialization project in the autumn of 2018 [1]. The project was created in cooperation between the Department of Marine Technology (IMT), the consultancy company CFD Marine AS and myself, to best fit all our interests. The content and procedure were designed on the go, as none of us really knew how to attack the problem. The project description is presented in Appendix A. A poster of the project is attached in Appendix B.

During my six years at NTNU, I have finished a Bachelor's Degree Program in Mathematical Sciences, and I am now finishing my fifth year at Engineering & ICT. The third year of the Masters' program I had to choose a main profile, and chose ICT & Marine Technology simply because I love ocean technology with its marine environment. For my specialization I wanted something that could combine ICT, Marine Technology and Mathematics. Hydrodynamics, or more specifically Computational Fluid Dynamics, does this perfectly. The fact that I can use my education to the benefit of a more sustainable world is what engages me the most.

I would first like to show great appreciation to my supervisor at IMT, Associate Professor Håvard Holm, for guiding me through this thesis. Due to his experience guiding many students before me, he is always keeping a realistic sight of the work amount, and was making sure I did not drown along the way.

Secondly, I would like to thank my co-supervisor at CFD Marine AS, Chief Executive Officer Hans Jørgen Bjelke Mørch, for the opportunity to work with such an encouraging and talented man and company. A phone call to him with any software problems or theoretical questions is always giving a motivation boost.

Finally, I would like to give big thanks to my fiancé, PhD Candidate at the Department of Mathematical Sciences at NTNU Are Austad, for helping me with general understanding of problem solving through my studies, and for always believing in me and encouraging me to work hard and stay strong.

<div align="right">

Hannelore Olsen

Hannelore Olsen

NTNU Trondheim

June 5, 2019

</div>

Summary

An increasing world population has created the problem of providing food and livelihood to all in a sustainable way. It is believed that aquaculture will be the fastest growing and most important animal-food sector in achieving this. The current production platforms, based on open systems, are too weak to sustain significant growth, recognized environmental performance and societal expectations. Therefore, new aquaculture technology, for instance closed fish farming cages, are being developed. To be able to control the environmental factors inside a closed fish farming cage, detailed flow calculations are needed. Computational Fluid Dynamics (CFD) methods replace model testing to be more time and cost efficient. The calculations are done, however, without considering how the motion of fish will affect the flow inside the systems. Whether fish in closed fish farming cages will reduce, increase or do nothing to the flow velocity of the surrounding water is a topic of discussion. How do fish affect the surrounding water? Is it okay to neglect the effects from fish when analyzing the flow in closed fish farming cages? How are the results compared to the literature? These are questions we have been asking ourselves through the scientific research done in this thesis.

Stepwise CFD simulations of fish and its surrounding flow have been conducted to identify if the effects from fish in closed fish farming cages are negligible. Each step in the CFD approach builds upon the reliability and validity of the previous one. It is found that STAR-CCM+ simulates the laminar and turbulent boundary layer over a flat smooth plate in parallel flow with high accuracy. The implementation of the fish motion also turned out to be of good correspondence to the equation for its motion. It is concluded that fish are affecting the flow in closed fish farming cages by increasing the pressure for higher fish density and smaller system. This implies that the fish biomass will reduce the velocity in a system of constant pressure, which is supported by the literature. Whether the effects are negligible is not possible to say until further investigation has been conducted.

Contents

1. Introduction

This thesis builds upon the review and preparation study done during the specialization project of autumn 2018 [1]. The specialization project considered a literature review of fish hydrodynamics, a stakeholder survey about the industry interest in computational fluid dynamics (CFD) around fish in aquaculture systems, and a simple CFD case study of the laminar boundary layer over a flat plate.

The background, problem statement and objectives, some previous work and state of the research field will be presented in this chapter. As the background is rather general, parts of it was also used for the specialization project. Significance of the work, scope and limitations, along with the overall structure of the report will be considered.

1.1 Background

"There is no plan B, because we do not have a planet B!" was the thought United Nations (UN) Secretary General Ban Ki-moon used to inspire world leaders in his speech at Climate Week NYC Opening Day held September 22, 2014 [2]. He described climate change as *"the defining issue of our time"*. This Climate Week guided the development of the 17 Sustainable Development Goals (SDGs) through the next year. 193 countries of the UN General Assembly adopted the 2030 Agenda "Transforming our world: the 2030 Agenda for Sustainable Development" in September 2015.

The term *sustainable* is about taking care of the needs humans have today, without compromising of future generations [3]. In a sustainable community there is balance between social, economical and environmental relationships. The SDGs are created to help us achieve this balance. *"We resolve, between now and 2030, to end poverty and hunger everywhere; to combat inequalities within and among countries; to build peaceful, just and inclusive societies; to protect human rights and promote gender equality and the empowerment of women and girls; and to ensure the lasting protection of the planet and its natural resources. We resolve also to create conditions for sustainable, inclusive and sustained economic growth, shared prosperity and decent work for all, taking into account different levels of national development and capacities"* [4].

According to the UN [5], the current world population of 7.6 billion people is expected to reach 8.6 billion in 2030, and almost 10 billion in 2050. Human society face an enormous challenge of having to provide food and livelihood to this population, while addressing the disproportionate impacts of climate change and environmental degradation on the resource base. Even though earth's surface is 75 % ocean, only 2 % of our total calorie intake is seafood. The State of World Fisheries and Aquaculture 2018 [6] claims that food and agriculture are key to achieving the entire set of SDGs, where fisheries and aquaculture has direct relation to SDGs 14, 2, 8, 9 and 12, shown in Figure 1.1. As of 2016, an all-time record of 171 million

tonnes of fish were caught world wide, where 88 % went directly to human consumption. The total world fish production is expected to reach 201 million tonnes in 2030, a growth of 18 % over 2016. Despite a lower growth rate than observed the last 15 years, the production from aquaculture is expected to have a growth of 37 % over 2016. Aquaculture will be the fastest growing animal-food sectors, with 60 % of the global apparent food fish consumption in 2030, compared to 52 % in 2016 [6].

Figure 1.1: Sustainable Development Goals directly related to the aquaculture industry [6].

The open sea fish farming cages and net pens started the real growth of aquaculture in the 1970s and -80s [6]. This is still the most common way of doing fish farming today, and is considered simple, effective and cheap. The recent trend has been toward increasingly large diameter high density polyethylene (HDPE) collar cages, which are widely used in modern-industrial marine aquaculture in many parts of the world, and allow high density of fish [7]. However, there are many problems associated with open cage culture world wide. Feed must be nutritionally complete and kept fresh. There are often reduced dissolved oxygen and increase of ammonia concentration in and around the cage due to high density, stress, and high feeding rates, especially if there is no water movement through the cage. Wild fish can transmit diseases to the caged fish, and vice versa. Caged fish are easy targets for poachers and other predators, as for example bigger fish, turtles, snakes, otters, raccoons and birds. They take fish and/or damage the net, resulting in large escapes. In addition to these problems, it is difficult to overwinter warm water fish in cages, which usually results in high mortality rates [8].

The current production platform, based on open net pen systems, is too weak to sustain significant growth, recognized environmental performance and societal expectation, according to PwC Seafood Barometer 2017 [9]. To reduce the problems with open cages, research and development (R&D) on new aquaculture technologies is of big interest. Closed fish farming technologies will help to improve issues with diseases and parasites, escaping, poachers and local environmental conditions. The environment inside the cage will be under control, ensuring stable water flow, feeding and harvesting. This will reduce stress, diseases, low oxygen, and loss of uneaten food. Placing cages offshore in harder weather conditions will increase the number of cages and the density of fish in each unit, which will have a huge impact on sustainable growth. Closed recycling aquaculture systems (RAS) are already well developed technology and are used on land for young fish. These systems will possibly be seen in the future for adult fish as well, floating in the ocean [9].

To accelerate R&D within the field, the Norwegian Government, in cooperation with the Norwegian Directorate of Fisheries, have made a huge initiative. Between November 20,

2015, and November 17, 2017, it was open to apply for development licenses which were given to certain projects based on innovation and resource requirements within aquaculture technology [10]. This was a very popular initiative as each license is estimated to have a value of 100 MNOK [9]. There were 104 applications, where 85 of them have been rejected so far. 11 applications are issued, together for 68 licenses (50 770 tonnes), where 10 (5 780 tonnes) of these are for closed systems (May 11 2019) [10].

Detailed calculations and testing are needed to be able to control all factors inside a closed fish farming cage in order to see how the flow acts inside the system, and change the design to obtain optimal conditions. This can be done by model experiments and measurements, or by CFD and theory. CFD has been used frequently in the applications for development licenses to calculate the flow inside closed fish farming cages. However, the calculations are done by neglecting the biomass, and thereby the motion and effects the fish might have on the flow conditions inside the system.

1.2 Problem Statement and Objectives

Whether fish in closed fish farming cages will reduce, increase or do nothing to the flow velocity of the surrounding water is a topic of discussion. According to the stakeholder survey conducted in the specialization project [1] last semester, seven out of eight relevant replies had discussed the issue and where interested in hearing about the results. Based on this problem statement, the following questions are constructed:

1. How do fish affect the surrounding water?

2. Are the effects from fish negligible when analyzing the flow in closed fish farming cages?

3. How do the results compare to literature?

Thus, the objectives to answer these questions will be

- to conduct CFD simulations of fish and the surrounding flow,

- to identify what the effects from fish in closed fish farming cages are and if they can be neglected by analyzing the simulations,

- to compare the results of the study to results found in literature.

1.3 Previous Work

Numerical studies of fish and their hydrodynamics are numerous. Specific species, as tadpole- [11], dolphin- [12] and tuna-like swimming [13, 14, 15], have been investigated by means of CFD to understand their maneuvering and propulsion. Different kinematics and similar shapes (and vice versa) of anguiliform and carangiform fish have been investigated to look at the swimming efficiency depending on different parameters [16, 17, 18, 19, 20]. It is concluded that the wake structure and thereby the swimming efficiency is highly dependent on the Strouhal number, not the body form or kinematics. Hannon [21] compared free-stream and Kármán gait swimming and concluded that the Kármán gait in the presence of a Kármán vortex street was the most efficient swimming mode, corresponding to the literature.

More general fish hydrodynamic studies are also done to investigate the flow around and on fish with the interest in developing vehicles capable of emulating the high performance of fish propulsion and manoeuvring both in 2-D and 3-D [22, 23, 24, 25]. Parameters as drag and lift forces, swimming efficiency, spatial structure of the wake, and distribution of forces along the fish body have been measured. Adkins and Yan [22] concluded in 2006 that CFD methodology is a viable and powerful additional problem-solving tool in the field of bio-locomotion and biomimetics.

All these papers are focusing on the fish itself, and how/why the fish is swimming the way it is, and how it is affected by the flow. This study will assume a generic fish-like body swimming in viscous flow to see how the flow is affected by it, and how this will influence the overall flow environment in closed fish farming cages. Johansson *et al.* [26] concluded that in high current environment the traditional circular group structure switched to a structure where all fish kept stations at fixed positions swimming against the current. Based on this, it is interesting to discuss whether the motion in closed cages should be kept at such velocity that the fish is kept at fixed position swimming against the current, or if this is exhausting for the fish. Either way, we are interested in seeing how fish affect this given flow velocity. Gorle *et al.* [27] presented empirical data on rotational velocity and water quality in circular and octagonal tanks at two large commercial smolt production sites. The effect of biomass on the velocity distribution was examined, and the effect of operating conditions on the water quality was studied. The total biomass of the Atlantic salmon smolt in the cages were found to decrease the water velocity by up to 25 %.

1.4 Significance, Scope and Limitations

The findings of this study redound to the benefit of the society considering that it shows how CFD can be used in this research area, being a much more cost and time efficient methodology than for example model testing. Also, enormous resources have been given by the Norwegian Governance and Directorate of Fisheries for research and development of new fish farming technologies through development licenses. Thus, companies trying to develop the best and most sustainable designs for new closed systems can use the knowledge when calculating the conditions for the internal flow. CFD consultancy companies will be able to use the knowledge from this study to provide more accurate calculations for their costumers, which might contribute to even better designs.

The thesis will serve as a research study to create new generic knowledge considering how the presence of fish affects the surrounding flow in closed fish farming cages. Many assumptions will have to be made, as a randomly swimming fish is a very complex case to simulate. The study will focus on 2-D fish with a given swimming function in constant incoming flow to look at the theoretical details on this case instead of rushing forward to look at complex 3-D cases without being able to give good analyses. It is limited to a computational study, and will not include any model experiments. The reliability and validity of the simulated results will be discussed in comparison with the literature.

1.5 Organization of the Report

Included in this thesis are 7 chapters. Chapter 2 will consider the theory included in fish hydrodynamics and the basics of computational fluid dynamics. Chapter 3 will cover the methodologies and methods used in the thesis including a short overview of the computer equipment and procedure. A detailed review on how the simulations were prepared, run and analyzed will be presented in Chapter 4. The results will be presented in Chapter 5 and discussed in Chapter 6. Chapter 7 will give some conclusions, recommendations and suggestions for further work.

2. Theory

The theory needed to follow the coming research study will be presented in this chapter. Some theory on fish hydrodynamics will come first, followed by general theory behind any CFD study. Section 2.1, 2.2.1 and 2.2.5 are mostly reused from the specialization project [1].

2.1 Fish Hydrodynamics

Natural selection has ensured that the mechanical systems evolved in fish, although not necessarily optimal, are highly efficient with regard to the habitat and mode of life for each species. These characteristics are inspiring innovative designs to improve the designs of marine autonomous vehicles and other systems operating in the aquatic environment. 85 % of fish species primarily use body and/or caudal fin (BCF) to generate thrust. The others use median and/or paired fin (MPF) propulsion [28]. The focus of this thesis will be on BCF swimmers. These are the high speed, high efficiency and high mobility fish generating thrust through a wave travelling from head to tail, which is how the typical farmed fish is.

Based on the body parts that are displaced laterally, BCF swimming can be divided into (a) anguilliform, *i.e.* eel types, (b) subcarangiform, *i.e.* salmonids, (c) carangiform, *i.e.* pelagic types, and (d) thunniform, *i.e.* tunas [29]. The swimming styles (a) through (d) are illustrated in Figure 2.1.
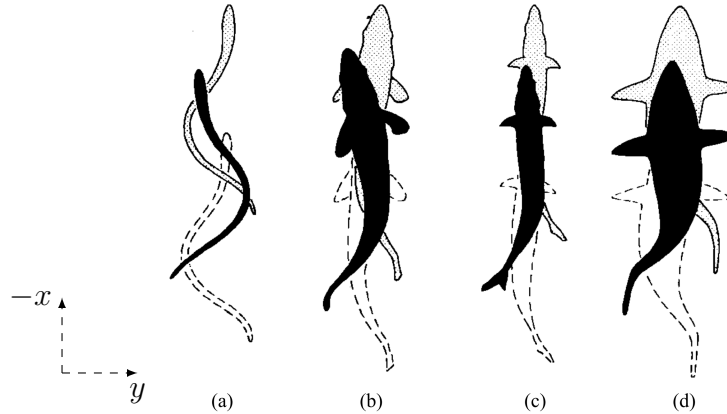

Figure 2.1: BCF swimming styles (a) anguilliform, (b) subcarangiform, (c) carangiform and (d) thunniform (Lindsey [29]).

Subcarangiform and carangiform fish are often collected to one category. This category of carangiform swimming style will be the focus through this thesis because it is the typical farmed fish in Norway. The parameterized kinematics law of BCF motions can according to Videler [30] be described as

$$y(x,t) = a(x)\sin(kx - \omega t), \tag{2.1}$$

where $y(x,t)$ represents the midline motion of fish body at body point x and time t, ω is

the tail-beat frequency, and k is the wave number. The function $a(x)$ is a function for the amplitude defined for carangiform [30] as

$$a(x) = a_1 + a_2 x + a_3 x^2, \tag{2.2}$$

where the constants a_1, a_2 and a_3 are quadratic coefficients of the amplitude envelope. The cross-section of carangiform fish can be defined as an ellipse, where the profiles of the half-height $R(x)$ and the half-width $r(x)$ according to Alvarado [31] can be expressed as

$$R(x) = 0.14L \sin\left(\frac{2\pi}{1.6L}x\right) + 0.0008L\left(e^{\frac{2\pi}{1.1L}x} - 1\right) \tag{2.3}$$

and

$$r(x) = 0.045L \sin\left(\frac{2\pi}{1.25L}x\right) + 0.06L\left(e^{\frac{2\pi}{3.14L}x} - 1\right), \tag{2.4}$$

where L is the total fish length.

2.1.1 Forces

The incomprehensibility and high density of water are key characteristics as the momentum from the fish transfers to the surrounding water (and vice versa), and the buoyancy nearly counteracts the force of gravity from the fish. The main momentum transfer mechanics are via drag (viscous and pressure forces), lift, and acceleration forces. The forces acting on a swimming fish are therefore weight, buoyancy, hydrodynamic lift, thrust and resistance [28], and are illustrated in Figure 2.2. If the total forces in x-direction is equal to zero, the fish is standing still, or having the same opposite velocity as the water.
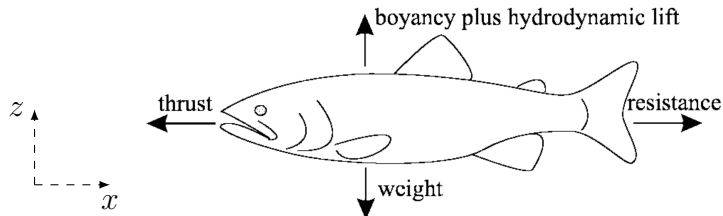

Figure 2.2: Forces acting on swimming fish (Lane *et al.* [28]).

For a fish propelling itself at constant speed, the momentum conservation principle requires that the forces and moments acting on it are balanced. Therefore, the total thrust it exerts against the water has to equal the total resistance it encounters moving forward. One of the main factors determining the relative contribution of the momentum transfer mechanisms to thrust and resistance is the ratio of inertial over viscous effects, the Reynolds number,

$$Re = \frac{LU}{\nu}, \tag{2.5}$$

where U is the swimming velocity and ν is the kinematic viscosity of water. Re is typically in the range of $10^3 < Re < 5 \cdot 10^6$ for adult fish, which is the range where inertial forces are dominant [28], as illustrated in Figure 2.3. In still water, boundary layer profile shape always suggests laminar flow of the carangiform swimmer Stenotomus chrysops (Scup) according to

Anderson *et al.* [32], looking at Reynolds number in the range of $3 \cdot 10^3 < Re < 3 \cdot 10^5$. In flowing water, however, the boundary layer profile shape suggests laminar flow at the lower numbers, and turbulent flow at the highest numbers.
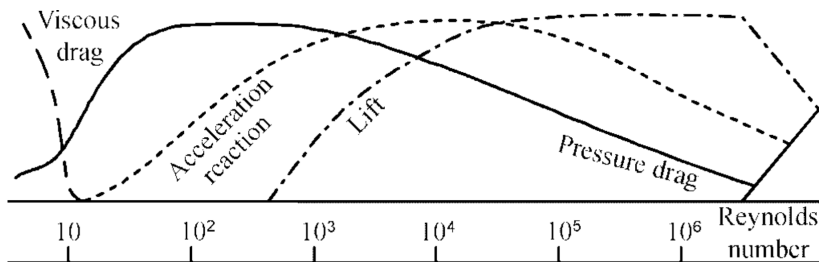

Figure 2.3: Relative contribution of moments transfer mechanism for swimming vertebrates, plotted against Re (Webb [33]).

2.1.2 Propulsion

The propulsive wave generated through the fish body traverses the fish in a direction opposite to the overall movement, with a higher speed than the overall swimming speed. The ratio U/V, where U is the overall swimming speed and V is the propagation speed, has long been used to indicate the swimming efficiency [28].

Flexing the body to achieve propulsion is expected to increase viscous drag by a factor of q compared to an equivalent rigid body. This is called a "boundary layer thinning" effect as the increased velocity gradients and hence the shear stress is due to lateral body movement reducing the boundary layer. What q is, has been discussed in several papers, without any agreement [33, 11, 34, 35], and depends on fish species and size. Swimming viscous drag is calculated using the standard Newtonian equation [28]

$$\vec{F} = \frac{d\vec{p}}{dt} \tag{2.6}$$

to get

$$F_D = \frac{1}{2}C_D S U^2 \rho. \tag{2.7}$$

Here C_D is the drag coefficient, depending on Re, the nature of the flow and the roughness of the fish. Further, S is the wetted surface area, and ρ is the water density.

Behind BCF swimmers is a wake of staggered array of trailing discrete vortices of alternating directions, generated by the tail movement. The vortices has opposite sign to the drag-producing Bénard-von Kármán (BvK) vortex street, a so-called reversed Bénard-von Kármán (rBvK) vortex street [11]. This generates a thrust force, not a drag force, as it for example does for a circular cylinder. This is illustrated in Figure 2.4. The ratio of unsteady to inertial forces, the Stouhal number,

$$St = \frac{fA}{U}, \tag{2.8}$$

is the parameter characterizing the structure of such wakes, with A the wake width and $f = \omega/2\pi$ tail beat frequency in hertz. Triantafyllou *et al.* [36] concluded that for oscillating foils, a Strouhal number in the range of $0.25 < St < 0.4$ would optimize the generated thrust.

More recently, Eloy [37] established the Strouhal number for 53 different species of aquatic animals, showing that the optimal one is in the range to $0.15 < St < 0.8$.
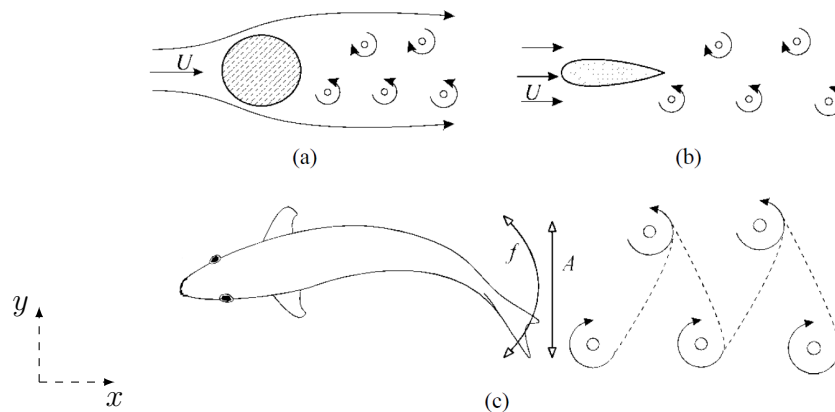
Figure 2.4: Kármán street (BvK) generating drag for (a) bluff and (b) streamlined body, but reversed Kármán (rBvK) generating thrust for (c) swimming streamlined body (Lane *et al.* [28]).

On the sides of the vortex street behind the fish, a water motion occurs in the swimming direction. In the middle of the vortex street the water motion is in the opposite swimming direction. A fish situated laterally midway between two fish will therefore avoid having to overcome increased income flow, and can utilize this favorable flow. This creates a diamond-shape pattern as the basic optimum structure in fish schools, with a distance H between two fish in the same column as illustrated in Figure 2.5. The average energy saved from schooling is 10–20 % [38].
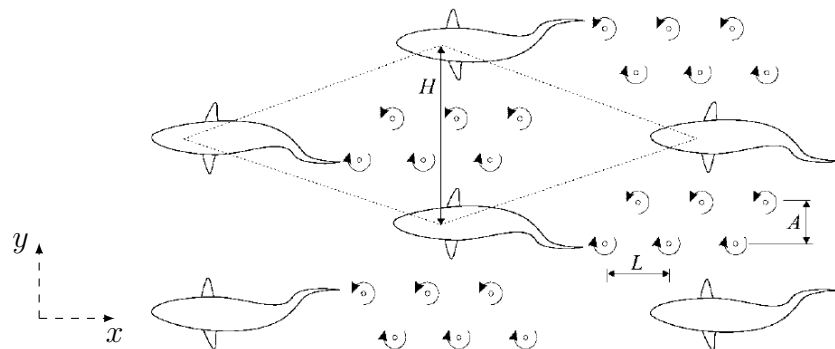
Figure 2.5: Diamond-shaped structure in fish schools when utilizing the favorable flow on the sides of the vortex streets (Weihs and Webb [38]).

2.2 Computational Fluid Dynamics

CFD is a branch of fluid dynamics that uses numerical analysis and data structures to simulate interactions between fluids and surfaces, defined by boundary conditions. This is done by solving partial differential equations (PDEs) with discrete methods due to the nature of computing. The progress in CFD the last years has been enormous [39], with applications in for example electronics, turbo machinery, power and energy, construction, hydraulics, vehicles on roads, at sea and in air, sports, biology and medicine. In all approaches, the procedure is the following:

1. Preprocessing; defining the geometry, mesh, physical models and boundary conditions.

2. Simulating; solving the equations iteratively.

3. Postprocessing; visualizing and analyzing the solution.

2.2.1 Governing Equations

A PDE is a differential equation that contains unknown multivariable functions and their partial derivatives. PDEs can be used to describe a wide variety of phenomena such as sound, heat, electrostatics, electrodynamics, elasticity, quantum mechanics and fluids. Fluid dynamics is a branch of physics concerned with the mechanics of fluids (liquids, gases and plasma), and the forces on them. The usual problem is highly nonlinear, so governing PDEs form a nonlinear system that must be solved for the unknown pressure, densities, temperatures, and velocities.

In fluid dynamics there are three such fundamental equations based on three conservation laws; conservation of mass, momentum and energy [39]. They give rise to the continuity equation, the momentum equation and the energy equation, respectively. The fluid of interest is water, which is incompressible and Newtonian, and is assumed to have constant properties. This includes the temperature, which means that the energy equation will not be of interest.

The continuity equation states that the rate at which mass enters a system is equal to the rate at which mass leaves the system plus the accumulation of mass within the system. The differential form of the continuity equation is written as

$$\frac{\partial \rho}{\partial t} + \nabla \cdot (\rho \vec{u}) = 0, \tag{2.9}$$

where ρ is the fluid density, t is time, and $\vec{u}$ is the flow velocity vector field. The time derivative can be understood as the accumulation (or loss) of mass in the system, while the divergence term represents the difference in flow in versus flow out. With the assumptions made above, Equation 2.9 simplifies to

$$\nabla \cdot \vec{u} = 0. \tag{2.10}$$

The momentum equation is also known as the Navier–Stokes equations, and describes the motion of viscous fluid substances. These balance equations arise from applying Newton's second law in Equation (2.6) to fluid motion, together with the assumption that the stress in the fluid is the sum of a diffusing viscous term (proportional to the gradient of velocity) and a pressure term, hence describing viscous flow. The differential form of the Navier-Stokes equations for a Newtonian fluid is written as

$$\rho \left(\frac{\partial \vec{u}}{\partial t} + \vec{u} \cdot \nabla \vec{u} \right) = -\nabla p + \mu \nabla^2 \vec{u} + \vec{g}, \tag{2.11}$$

where p is the pressure, μ is the dynamic viscosity and $\vec{g}$ the body acceleration acting on the continuum.

2.2.2   Computational Domain

There are two ways of describing a flow [40]:

1. The Lagrangian description; individual fluid particles are "marked", and their positions, velocities, etc. are described as a function of time. However, fluid flow is a continuum phenomenon, at least down to the molecular level. It is not possible to track each "particle" in a complex flow field. The Lagrangian description is therefore rarely used in fluid mechanics. This is called a system analysis and is often used in thermodynamics and solid mechanics.

2. The Eulerian description; a control volume is defined, within which fluid flow properties of interest are expressed as fields. This is a so-called open system, where each property is expressed as a function of space and time, which is ideal for a complex fluid flow.

In a closed system, the size and shape may change during the process, but no mass crosses its boundaries. A control volume allows mass to flow in or out across its boundaries on the other hand. This is exactly what is done in a CFD simulation; boundary conditions are given, where the flow inside these boundaries is of interest, and the flow outside is irrelevant. This area, or this volume of control, is the computational domain where the flow is simulated. An example of a 2-D computational domain is shown in Figure 2.6. The domain can be completely arbitrary, in two or three dimensions, depending of the case of interest. Important characteristics of a control volume is that mass entering and mass leaving the system must balance each other. Combining this with the fact that fluid velocity is inversely proportional to fluid pressure will be important.
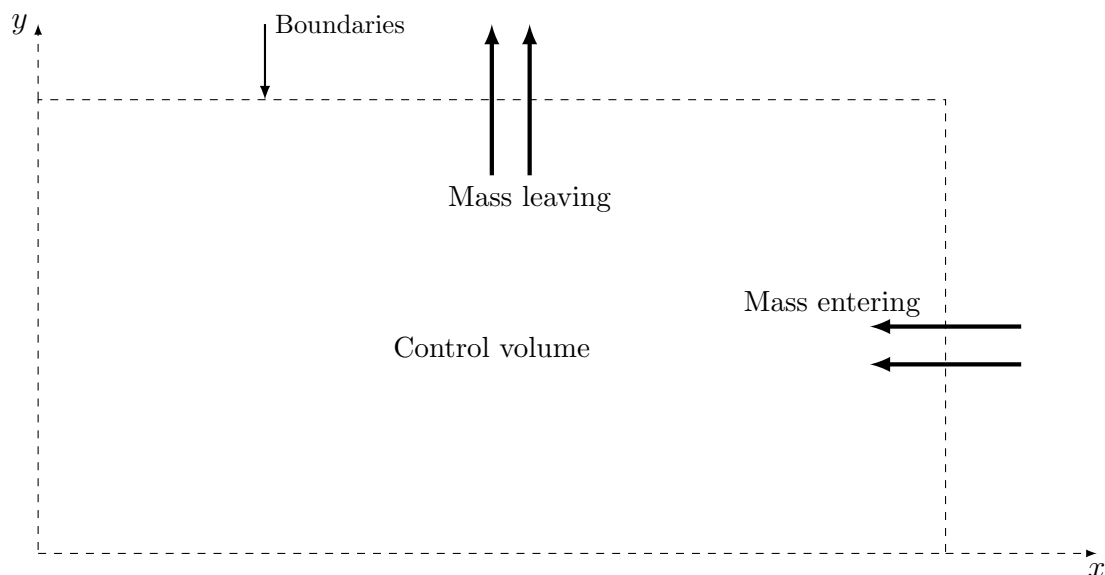

Figure 2.6: Example of computational domain in 2-D.

2.2.3   Discretization Process

The central process in CFD is discretization, *i.e.* the process of taking PDEs with infinitely many degrees of freedom and reducing them to a system of finitely many degrees of freedom. Hence, instead of determining the solution everywhere and for all times, the calculation at

a finite number of locations and at specified time intervals will be considered. The PDEs are then reduced to a system of algebraic equations that can be solved on a computer. The nature and characteristics of the errors must be controlled in order to ensure that the correct equations are solved (consistency property), and that the error can be decreased as the number of degrees of freedom is increased (stability and convergence). Once these criteria are established, the power of computing machines can be leveraged to solve the problem in a numerically reliable fashion.

Spatial Discretization

Various spatial discretization schemes have been developed to cope with a variety of issues. The finite volume method (FVM) is the most common in the context of CFD [41]. The first step in the solution process with FVM is discretizing the geometric domain into non-overlapping volume elements. The PDEs are then discretized into equations by integrating them over each discrete element. The system of equations is then solved to compute the values of the dependent variable for each of the elements [42].

In the FVM some of the terms in the conservation equation are turned into face fluxes and evaluated at the element faces. Because the flux entering a given volume is identical to that leaving the adjacent volume, the FVM is strictly conservative, which makes it the preferred method in CFD. Another important attribute of the FVM is that it can be formulated in the physical space on unstructured polygonal meshes. Finally, it is quite easy to implement a variety of boundary conditions in a non-invasive manner, when the unknown variables are evaluated at the centre of the volume elements and not at their boundary faces.

These characteristics have made the FVM quite suitable for the numerical simulation of a variety of applications involving fluid flow, and heat and mass transfer. Developments in the method have been closely intertwined with advances in CFD. From a limited potential at inception confined to solving simple physics and geometry over structured grids, the FVM is now capable of dealing with all kinds of complex physics and applications.

Temporal Discretization

Temporal discretization involves the integration of every term in the governing equations over a time step Δt. First, values at a given control volume at time interval t are assumed and then the values at time interval $t + \Delta t$ is found. This method states that the time integral of a given variable is equal to a weighted average between current and future values. After discretizing the time derivative, it remains to be evaluated. This can be done using implicit (at a future time) and explicit (at the current time) integration.

2.2.4 Turbulence Modeling

There are two qualitatively different types of viscous fluid flows; laminar and turbulent. Turbulent flows are characterized mainly by unsteadiness, vorticity, three-dimensionality, dissipation, wide spectrum of scales, and large mixing rates. The outstanding feature of turbulent flow, as opposed to laminar flow, is that the molecules move in a chaotic fashion along complex irregular paths. The strong chaotic motion causes various layers of fluid to mix together intensely. Because of the increased momentum and energy exchange between

the molecules and solid walls, turbulent flow leads to higher skin friction and heat transfer compared to laminar flow.

The solution of the Navier-Stokes equations does not raise any fundamental difficulties in the case of laminar flows. However, the simulation of turbulent flows still constitutes a significant challenge. Despite the performance of modern supercomputers, a direct simulation of turbulence by the time-dependent Navier-Stokes equations (2.11), known as the direct numerical simulation (DNS), is applicable only to relatively simple flow problems at low Reynolds numbers *i.e.* around 10^4–10^5. A more widespread utilization of the DNS is prevented by the fact that the number of grid points needed for sufficient spatial resolution scales as $Re^{9/4}$ and the CPU-time as Re^3 [42].

It is forced to account for the effects of turbulence in an approximate manner due to this scaling of CPU-time. A large variety of turbulence models have been developed, and the research is still highly relevant. A model hierarchy by Xiao and Cinnella [43] shows the top representing the most physics-resolving and computationally expensive approach (DNS), and the most empirical and computationally affordable approach (RANS) at the bottom in Figure 2.7. The theory behind approximating treatment of turbulent flows is huge and complex, therefore only a small written review of the procedure will be presented. For a more mathematical approach of turbulence modelling, see Chapter 7 in [42].
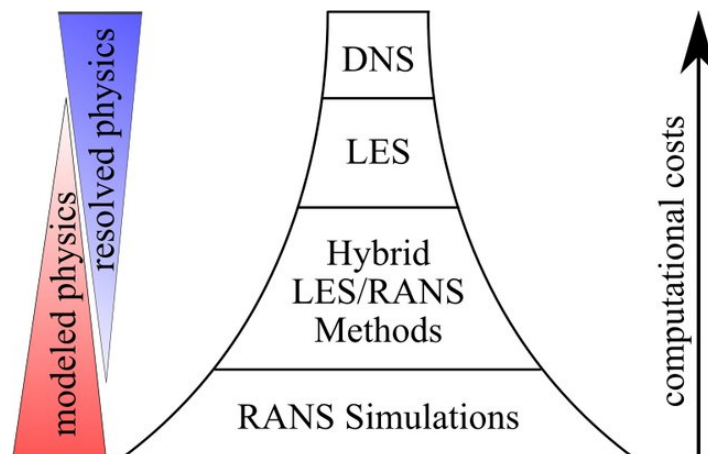

Figure 2.7: A schematic representation of the hierarchy of turbulence modeling approaches based on computational costs and the amounts of resolved versus modeled physics (Xiao and Cinnella [43]).

Reynolds-Averaged Navier-Stokes Equations

The first approach for the approximate treatment of turbulent flows was presented by Reynolds in 1895, and is still commonly used [44]. The methodology is based on the decomposition of the flow variables into a mean and a fluctuating part, so-called Reynolds averaging. The governing equations are then solved for the mean values, which are very interesting for engineering applications. If we apply the Reynolds averaging to the Navier-Stokes equations, adding a Reynolds stress tensor, we get the Reynolds-averaged Navier-Stokes (RANS) equations. The stress tensor represents the transfer of momentum due to turbulent fluctuations, and consists of six independent components (out of nine elements). Thus, the fundamental

problem is to find six additional relations in order to close the RANS equations [44].

The first-order closures, which represents algebraic, one- and multiple equations, represent the easiest way to approximate the Reynolds stresses in the Reynolds averaged Navier-Stokes equations. They are based on Boussinesq or non-linear eddy-viscosity models [44]. Boussinesq's idea is based on the observation that the momentum transfer in a turbulent flow is dominated by the mixing caused by large energetic turbulent eddies. It assumes that the turbulent shear stress depends linearly on the mean rate of strain, as in a laminar flow, with the eddy-viscosity as the proportionality factor. In order to remove the restrictions imposed by the assumption of equilibrium between the turbulence and the mean strain rate, Lumley proposed to extend the linear Boussinesq approach by higher-order products of strain and rotation tensors. This can be viewed as a Taylor series expansion. Following the idea of Lumley, numerous non-linear eddy-viscosity models were proposed. Once the eddy-viscosity is known, the Navier-Stokes equations can easily be extended to the simulation of turbulent flows by introducing averaged flow variables and by adding μ_T to the laminar viscosity [44]. Consequently, the task of an associated turbulence model is to compute the eddy-viscosity μ_T.

K-epsilon (k-ε) turbulence models are the most common models used in CFD to simulate mean flow characteristics for turbulent flow conditions. They are so-called *two-equation models* that gives a general description of turbulence by means of two transport equations (PDEs). The first transported variable is the turbulence kinetic energy k, and the second is the rate of dissipation of turbulence energy ε [44]. The underlying assumption of these models is that the turbulent viscosity is isotropic, *i.e.* the ratio between Reynolds stress and mean rate of deformations is the same in all directions. The models have been tailored specifically for planar shear layers and recirculating flows. They have applications ranging from industrial to environmental flows, which explains the popularity. They are usually useful for free-shear layer flows with relatively small pressure gradients as well as in confined flows where the Reynolds shear stresses are most important. They can also be stated as the simplest turbulence models for which only initial and/or boundary conditions needs to be supplied.

The K-omega (k-ω) turbulence models are other common two-equation turbulence models in CFD. The first transported variable is the turbulence kinetic energy k, and the second is the specific rate of dissipation of the turbulence kinetic energy into internal thermal energy ω [44].

Large Eddy Simulations

A second approach for the approximate treatment of turbulent flows is large eddy simulations (LES). It is a compromise between DNS and RANS simulations at two ends of the spectrum. It resolves only the larger, more energetic scales, and models the smaller scales.

The methodology was employed already in 1963 by Smagorinsky in meteorology [45]. The first engineering application of LES (turbulent channel flow) was presented by Deardorff in 1970. His method was later extended and improved by Schumann. During 1980s, the research

focus in the simulation of turbulence shifted from LES to DNS. The interest in LES returned back at the beginning of 1990s. Nowadays, LES is increasingly employed for physically and geometrically complex flows of engineering relevance [45]. Certainly, this trend is supported by the availability of low-cost, highly powerful compute servers. Furthermore, in certain cases the mean flow frequencies are in the same order as the turbulent fluctuations. Hence, the time averaging loses its validity and we have to resort to either LES or to DNS.

Detached Eddy Simulations

Detached eddy simulations (DES) is a third approach of turbulence modeling. It is a hybrid modelling approach that combines features of RANS simulation in some parts of the flow and LES in others. The user gets the best of both worlds; a RANS simulation in the boundary layers and an LES simulation in the unsteady separated regions.

2.2.5 Boundary Layers

To be able to say something about the reliability of the results of a CFD simulation, it is crucial that it can be compared and supported by the literature. Fundamental case examples have been solved many times, and are therefore excellent for comparison. In the case of fish, it is really just a flat plate with motion, thickness and height. Therefore, the laminar boundary layer over a flat plate is an excellent case to compare with.

If a flow is assumed to be 2-D and steady in addition to the assumptions made in Section 2.2.1, Equation (2.10) can be written out as

$$\frac{\partial u}{\partial x} + \frac{\partial v}{\partial y} = 0, \tag{2.12}$$

and Equation (2.11) as

$$x\text{-component: } u\frac{\partial u}{\partial x} + v\frac{\partial u}{\partial y} = -\frac{1}{\rho}\frac{\partial p}{\partial x} + \nu\left(\frac{\partial^2 u}{\partial x^2} + \frac{\partial^2 u}{\partial y^2}\right) \text{ and,} \tag{2.13}$$

$$y\text{-component: } u\frac{\partial v}{\partial x} + v\frac{\partial v}{\partial y} = -\frac{1}{\rho}\frac{\partial p}{\partial x} + \nu\left(\frac{\partial^2 v}{\partial x^2} + \frac{\partial^2 v}{\partial y^2}\right). \tag{2.14}$$

Here, x and y are the horizontal and vertical coordinates, respectively, u and v are the horizontal and vertical fluid velocities, and p is the fluid pressure. Further, gravity is neglected, and the radius of the curvature is large, *i.e.* centrifugal forces are neglected to ensure no flow separation.

When fluid flows past a submerged body, *e.g.* a fish, a thin boundary layer will develop near the solid surface due to the no-slip condition. In this boundary layer, viscous effects play an important role, whereas outside the boundary layer the fluid can be considered inviscid. From Equation (2.10)–(2.14), and with some help from Bernoulli's equation, the boundary layer equations for laminar flow (not applicable for backflow) can be derived. As the boundary layer is assumed to be very thin, the pressure does not vary normal to the surface. Hence the boundary layer equations for laminar flow are stated as Equation (2.10) and Equation

(2.13), together with

$$\frac{\partial p}{\partial y} = 0,$$

(2.15)

and

$$\frac{1}{\rho}\frac{\partial p}{\partial x} = -u\frac{\partial u}{\partial x}.$$

(2.16)

For a flat plate with incoming flow of constant speed U, the laminar boundary layer over the flat plate can be found by solving these equations for u, v, and p simultaneously. By assuming uniform flow, we have that $\frac{\partial u}{\partial x} = 0$, and thereby Equation (2.16) implies that there is no pressure variation in x. By also considering Equation (2.15), the pressure is constant everywhere. Equation (2.13) is reduced to

$$u\frac{\partial u}{\partial x} + v\frac{\partial u}{\partial y} = -\frac{1}{\rho}\frac{\partial p}{\partial x} + \nu\frac{\partial^2 u}{\partial y^2}.$$

(2.17)

By the impermeability condition, the first boundary condition (BC) close to the plate becomes

$$v = 0 \text{ at } y = 0.$$

(2.18)

Due to viscosity the no-slip conditions holds at the plate, and the second BC becomes

$$u = 0 \text{ at } y = 0.$$

(2.19)

When moving away from the plate, we know that the horizontal velocity will reach the same velocity as the the incoming flow, which means that

$$u = U \text{ at } y = \infty$$

(2.20)

becomes the third and final BC.

This problem was solved by Blasius [46] by using a coordinate transformation ending in

$$\frac{u}{U} = g(\eta)$$

(2.21)

where

$$\eta = y\left(\frac{U}{\nu x}\right)^{1/2}$$

(2.22)

is a change of variable. The function g is a power series, and the solution was obtained by formulating a power series expansion about $\eta = 0$ and matching with an asymptotic solution about $\eta = \infty$. The boundary layer thickness δ is selected at the y-location where $u = 0.99U$. This occurs when $\eta \approx 5$, and the boundary layer thickness thereby can be expressed as

$$\eta = \delta\left(\frac{U}{\nu x}\right)^{1/2} = 5 \implies \delta = \frac{5x}{(Ux^2/\nu x)^{1/2}} = \frac{5x}{\sqrt{Re}}.$$

(2.23)

The skin friction coefficient is defined by Blasius as

$$C_f = \frac{0.664}{\sqrt{Re_x}}.$$ (2.24)

It is possible to estimate quantities of interest, such as the 99% boundary layer thickness and the local skin friction coefficient also for turbulent boundary layers. The derivation of these are however beyond the scope of this thesis. The expressions are summarized in Table 2.1. The expressions in the 'Turbulent (a)" column is obtained from one-seventh-power law combined with empirical data for turbulent flow through smooth pipes. These values are in general preferred for engineering analyses. The expressions in the "Turbulent (b)" column is based on Prantl's approximation, obtained from one-seventh-power law [40]. Laminar values are exact and are listed to three significant digits, but turbulent values are listed to two significant digits due to the large uncertainty affiliated with all turbulent flow fields [40].

Table 2.1: Expressions for laminar and turbulent boundary layers on a smooth flat plate aligned parallel to a uniform flow [40]. (a) obtained from one-seventh-power law combined with empirical data for turbulent flow through smooth pipes. (b) obtained from one-seventh-power law.

Parameter	Blasius' Laminar	Turbulent (a)	Turbulent (b)
Boundary layer thickness δ	$\frac{5x}{\sqrt{Re_x}}$	$\frac{0.38x}{Re_x^{1/5}}$	$\frac{0.16x}{Re_x^{1/7}}$
Skin friction coefficient C_f	$\frac{0.664}{\sqrt{Re_x}}$	$\frac{0.059}{Re_x^{1/5}}$	$\frac{0.027}{Re_x^{1/7}}$

2.2.6 Uncertainty and Error

Uncertainties and errors that cause CFD simulation results to differ from their true or exact values are not only applicable to CFD code, but other computer programs used in the analysis process such as CAD packages, grid generators, and flow visualizers. Uncertainty is defined as *"A potential deficiency in any phase or activity of the modeling process that is due to the lack of knowledge"* [47]. Error is defined as *"A recognizable deficiency in any phase or activity of modeling and simulation that is not due to lack of knowledge"* [47]. Error can be further divided into

- Acknowledged error; physical approximation error (physical modeling and geometry modeling), computer round-off error, iterative convergence error and discretization error (spatial and temporal).

- Unacknowledged error; computer programming and usage error.

Physical Approximation Error

Physical modeling errors are those due to uncertainty in the formulation of the model and deliberate simplifications of the model. Physical modeling errors are examined by performing validation studies that focus on certain models (*i.e.* inviscid flow, turbulent boundary layers, real-gas flows, etc.). Even when a physical process is known to a high level of accuracy, a

simplified model may be used within the CFD code for the convenience of a more efficient computation.

Computer round-off error

Computer round-off errors develops with the representation of floating point numbers on the computer and the accuracy at which numbers are stored. With advanced computer resources, numbers are typically stored with 16, 32, or 64 bits. Round-off errors are not considered significant when compared with other errors. If computer round-off errors are suspected of being significant, one test is to run the code at a higher precision or on a computer known to store floating point numbers at a higher precision.

Iterative Convergence Error

The iterative convergence error exists because the iterative methods used in the simulation must have a stopping point eventually. The error scales to the variation in the solution at the completion of the simulations.

Discretization Error

Discretization errors are those errors that occur from the representation of the governing flow equations and other physical models as algebraic expressions in a discrete domain of space and time. It is also known as numerical error.

A consistent numerical method will approach the continuum representation of the equations and zero discretization error as the number of grid points increases and the size of the grid spacing tends to zero. As the mesh is refined, the solution should become less sensitive to the grid spacing and approach the continuum solution. This is grid convergence. The grid convergence study is a useful procedure for determining the level of discretization error existing in a CFD solution.

In fluid dynamics, the *law of the wall* states that the average velocity of a turbulent flow at a certain point is proportional to the logarithm of the distance from that point to the wall, or the boundary of the fluid region. It is denoted by y^+ and is the distance y to the wall, made dimensionless with the friction velocity u_T and kinematic viscosity ν. For boundary layers in adverse pressure gradients it is imperative to have a $y^+ \leq 1$ to correctly predict flow separation. This means that the boundary layer flow is resolved all the way down to the wall. This is obtained by a grid satisfyingly refined.

The same thinking also applies to the time step; the discretization error tends to zero as the time step size decreases. The Courant–Friedrichs–Lewy (CFL) condition is a condition for the stability of unstable numerical methods that model convection or wave phenomena. As such, it plays an important role in CFD. The CFL condition expresses that the distance that any information travels during the time step length within the mesh must be lower than the distance between mesh elements. In other words, information from a given cell or mesh element must propagate only to its immediate neighbors. It follows from the numerical diffusion coefficient discussion that for any explicit simple linear convection problem, the Courant number must be equal to or smaller than 1 to have small enough time step for a

stable solution.

For implicit schemes it is a bit different. If CFL> 1 the time step is so high that the fluid particles do not reside within a cell but jump and cross one or more cells over that (large) time step. This means a loss of accuracy, but the solution is still stable. Therefore, CFL≤ 1 is still meaningful if one uses an implicit scheme to prevent loss of accuracy in a steady-state solution.

Computer Programming Errors

Programming errors are "bugs" and mistakes made in programming or writing the code. They are the responsibility of the programmers. These type of errors are discovered by systematically performing verification studies of subprograms of the code and the entire code, reviewing the lines of code, and performing validation studies of the code. The programming errors should be removed from the code prior to release.

Usage Errors

Usage errors are due to the application of the code in a less-than-accurate or improper manner, and may show up as modeling and/or discretization errors. The user sets the models, grid, algorithm, and inputs used in a simulation, which then establishes the accuracy of the simulation. A converged solution may be obtained, however, the conclusions drawn from the simulation may be incorrect. The errors may not be as evident, such as proper choice of turbulence model parameters for separated flows with shocks. The potential for usage errors increases with an increased level of options available in a CFD code. Usage errors are minimized through training and experience.

3. Methodology and Methods

The methodology, computer equipment, and the overall procedure of the research will be presented in this chapter. A detailed procedure description of the simulations themselves will come in Chapter 4.

3.1 Computational Methodology

As there are no previous studies on this problem, the study serves as ground work for developing a basis for future research within aquaculture technology, and is thereby an exploratory, applied and inductive research. To interpret results and keep them tangible is challenging in lack of comparison material, which makes this qualitative research.

Case studies are often described as exploratory research used in areas where there are few theories or definitions of body knowledge. The methodology used during this study thereby becomes a case study by means of CFD. This is a phenomenological research methodology as the main purpose is to examine a situation of interest.

CFD was chosen over experiments because of the interest in the industry and because experiments with fish requires a lot of equipment, fish, fish to do exactly what you want them to do etc. CFD is also an increasingly preferred methodology compared to experiments. It is more time and cost efficient as many simulations can be run to optimize a design before creating prototypes instead of testing several different prototypes. It is also very difficult to create the exact same environmental conditions and calibrations with experimental equipment.

3.2 Computer Equipment

The selected CFD software will be shortly presented followed by a short overview of the supportive software and hardware it was run on.

3.2.1 STAR-CCM+

The chosen CFD software for this thesis was STAR-CCM+ as it is used by CFD Marine AS, the company in which this thesis is written in cooperation with. To be able to receive proper and efficient guidance from them, this was an obvious choice. The license was distributed by the university.

STAR-CCM+ is a commercial all-in-one multidisciplinary software for the simulation of products and designs operating under real-world conditions. Ultimately, these results are of higher quality than hand calculations and experimental testing of physical prototypes, in a more cost efficient way [48]. By being able to test many designs, it is possible to exclude further investigation and model testing on those who prove to be useless already during the simulations. The software gives the possibility to run multidisciplinary simulations from a single

tool. This makes it ideal for a wide range of applications involving a lot of physics without having to worry about coupling different tools together. All the engineering disciplines included in the software are presented in Figure 3.1.
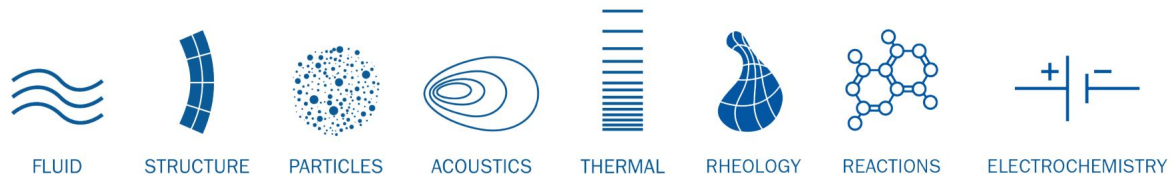
FLUID   STRUCTURE   PARTICLES   ACOUSTICS   THERMAL   RHEOLOGY   REACTIONS   ELECTROCHEMISTRY

Figure 3.1: STAR-CCM+ engineering disciplines.

The CFD capability in STAR-CCM+ offers an efficient and accurate set of fluid dynamics models and solvers with parallel performance and scalability. It provides a solid foundation for multidisciplinary design exploration:

- Coupled and segregated flow/energy solvers covering full range of applications from subsonic to hypersonic.

- Steady and unsteady implicit and explicit formulations allowing to pick the right solver for the right application.

- Wide range of turbulence models, from RANS to DES/LES, helping to account for turbulence on any scale.

- In-built porous media, fan and heat exchanger models for multidomain applications.

3.2.2 MATLAB

To look at curves, get values from functions, or to compare output from the simulation to theoretical values, MATLAB served as a support tool to STAR-CCM+. MATLAB is a multi-paradigm numerical computing environment and proprietary programming language developed by MathWorks. Matrix manipulations, plotting of functions and data, implementation of algorithms, creation of user interfaces, and interfacing with programs written in other languages, including C, C++, C#, Java, Fortran and Python, are the main features of MATLAB. It played a supportive role to the STAR-CCM+ during the whole thesis work period.

3.2.3 Hardware

There where two options when it came to hardware. One was to simulate directly on a HUAWEI MateBook X Pro, a PC powered by an 8th generation quad core Intel Core i5 processor. The other option was to connect externally to a server at CFD Marine AS. This made it however very difficult to follow the simulations while running them (to spot obvious mistakes early) as it was not possible to look at them locally while running them externally. A file to create videos from is made during simulations, which took hours to move back locally. Therefore, to be able to keep full attention to the simulation during running, the (possibly) more time consuming method of running them locally was chosen.

3.3 Procedure

To simulate biological phenomena requires assumptions and simplifications. The simulations were assumed to have constant incoming flow, parallel to the x-axis. The motion was given by a function giving a cyclic pattern. For validity and reliability reasons, the task was divided into three subtasks, where each task builds upon the validity and reliability of the previous one. The subtasks where called

1. fixed flat plate,

2. carangiform motion of thin plate,

3. 2D fish with carangiform motion.

A 2-D case study of the laminar boundary layer over a flat plate was conducted in STAR-CCM+ in the specialization project [1] in the autumn semester of 2018. The results were not as good as expected, and therefore more investigation had to be done before being able to move on. After some discussion between CFD Marine AS and the SIEMENS support service in London (distributer of STAR-CCM+), some possible reasons for the achieved results were discovered. It emerged that the 2-D simulations in STAR-CCM+ and the fact that there were no free flow in front of the plate had some rather essential impacts on the results. The old domain sketch is shown in Figure 3.2.
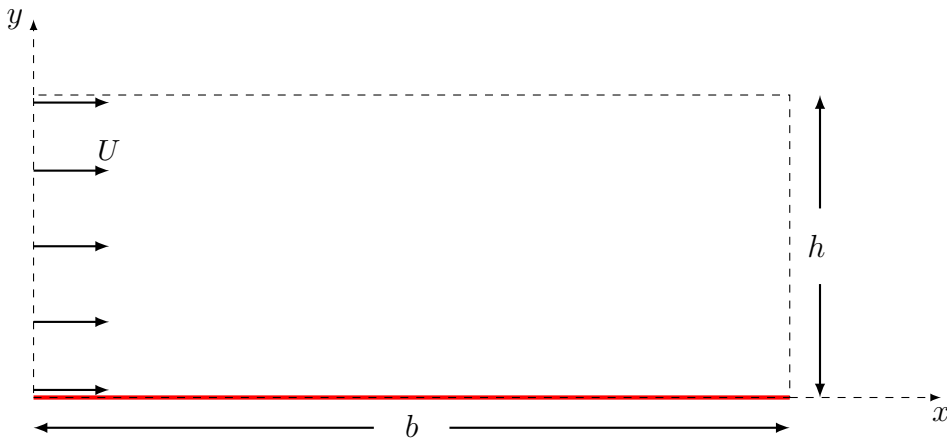
Figure 3.2: Old domain sketch of fixed flat plate with neither free flow in front of the plate (indicated in red) nor thickness in the z-direction. U is the flow velocity, b the domain width and h the domain height.

Based on this, some adjustments were done to get better groundwork to rely on. First, the plate was moved downwards the flow in x-direction. It was also moved to the center of the domain in y-direction as symmetry assumptions will no longer be valid after giving the plate motion further on. The domain was then transformed from 2-D to "semi" 2-D, *i.e.* with a small thickness of 0.002 m in the third dimension. The new domain sketch is shown in Figure 3.3 (a). The domain sketch of the plate with carangiform motion and the 2-D fish is shown in Figure 3.3 (b) and (c), respectively. The aim was to create a carangiform moving fish which was as close as possible to the typical farmed fish in Norway; Atlantic salmon.
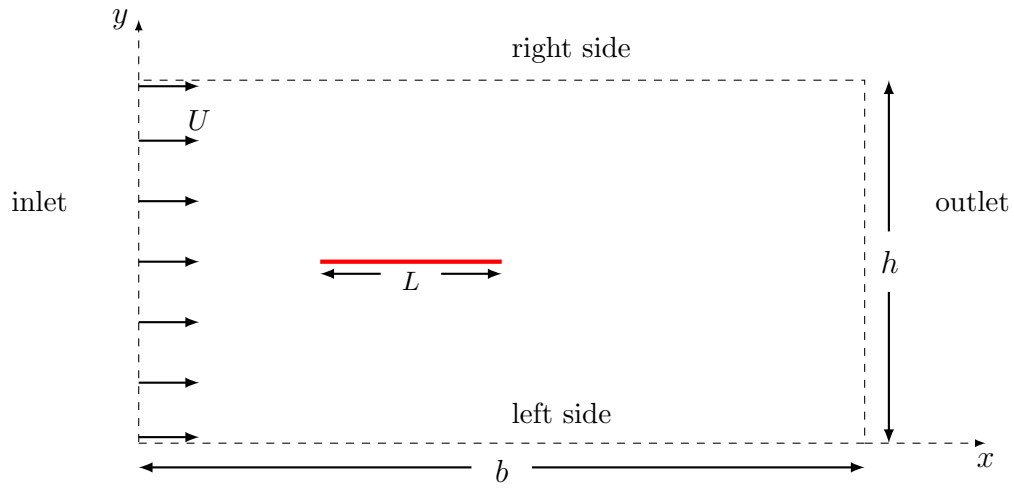
(a) New domain sketch of fixed flat plate
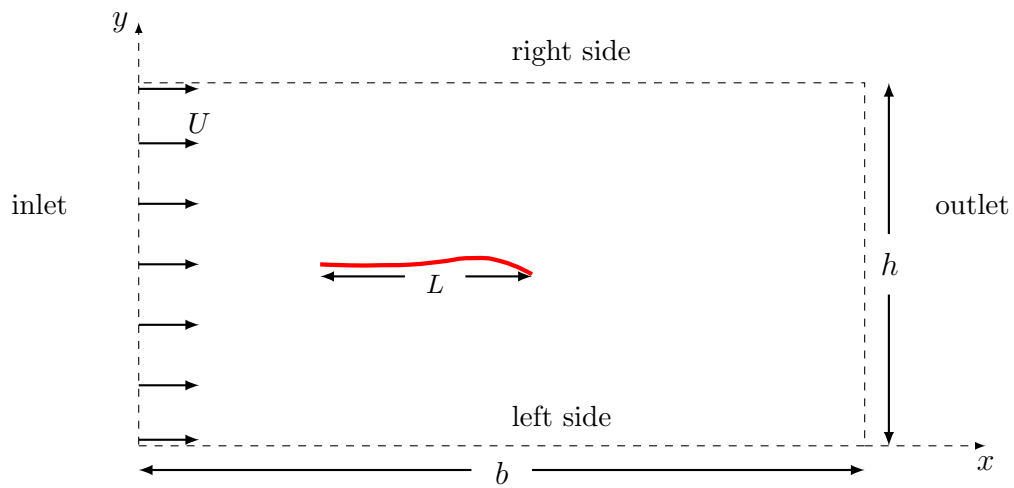
(b) Domain sketch of carangiform motion of thin plate in incoming flow
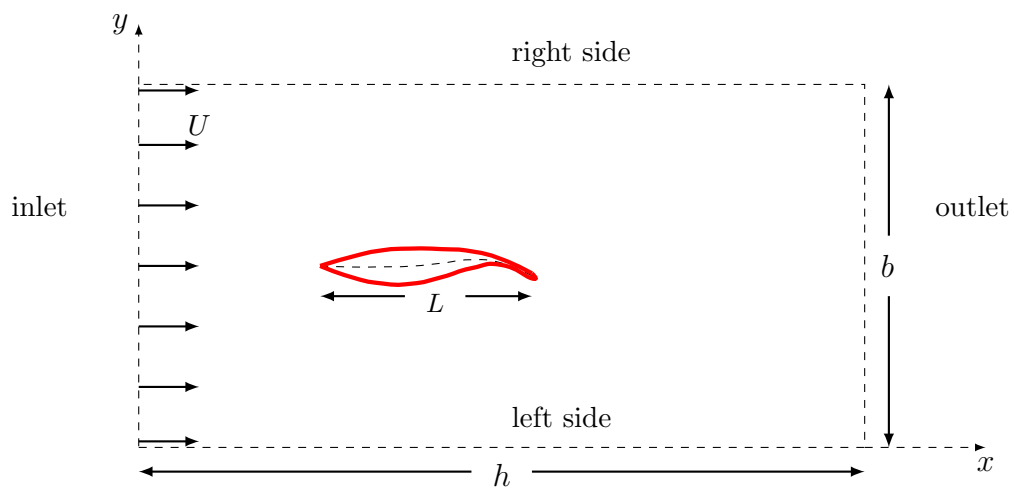
(c) Domain sketch of 2D fish with carangiform motion

Figure 3.3: Domain sketches of the three subtasks simulated during this CFD research study. U is the flow velocity, L the characteristic length, b the domain width and h the domain height. The inlet is where the water enters the domain and the outlet is where it leaves. The right and left sides are the sides of the domain which varies their conditions.

4. Simulating in STAR-CCM+

A detailed review of how the simulations were prepared, run and analyzed will be given in this chapter. The focus will be on presenting it in a manner such that the reader can recreate the simulations.

4.1 Preprocessing

Preparing a model for a simulation is called preprocessing. When preprocessing using STAR-CCM+ there are many things to think about depending on how advanced the case is. The following points are presented in an order to make sure that the preprocessing is done in a logical and efficient way. All the steps are done in such a way that they can be related to a carangiform moving fish which is as close as possible to the Atlantic salmon.

4.1.1 Geometry

The first step in preprocessing is always to create a geometry. This can be done either by importing a premade geometry, or by drawing in a 3-D computer-aided design (CAD) tool. A CAD tool is a part of STAR-CCM+, and was therefore the obvious choice. Creating the geometry for the flat plate was done by sketching a big rectangular volume of width $b = 4$ m, height $h = 2$ m and depth $d = 0.002$ m. A thin rectangle of 0.002 m width and 0.7 m length with a pointed end was cut out from the volume, representing the flat plate. The resulting volume represents the control volume for this case. The geometry is shown in Figure 4.1 (a), where the dimensions refers to the domain sketch in Figure 3.3 (a). The pointed end in front of the plate was made in order to reduce the effects from flow separation and rotations as much as possible. The front end of the plate is shown in a zoomed version of the geometry in Figure 4.1 (b).
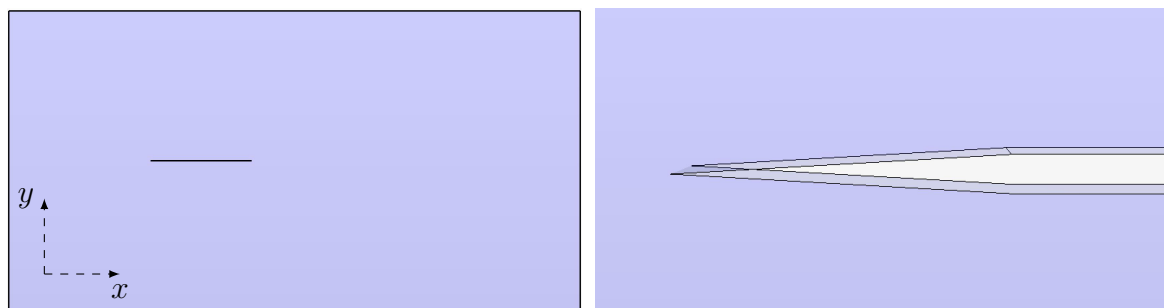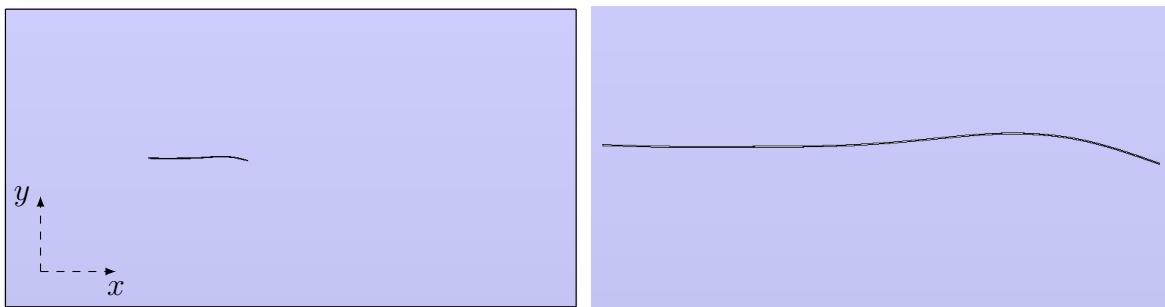

(a) The whole computational domain   **(b)** Zoomed in at the front end of the plate

Figure 4.1: Geometry of fixed flat plate. Referring to the domain sketch in Figure 2.6 (a), $b = 4$ m, $h = 2$ m and $L = 0.7$ m.

To give a carangiform shape to the plate, the initial position of the flat plate had to be changed. Values from Equation (2.1) at time $t = 0$ represents the midline of the fish, and

was used to create this carangiform plate. It was done by implementing the equation into MATLAB to get position values. These values were inserted as points in the CAD tool of STAR-CCM+, and a curved line (spline), was drawn between them. The geometry is shown in Figure 4.2, both the whole domain (a), and zoomed in at the carangiform plate (b). This subtask was created only to verify the carangiform motion, and was therefore not pointed at the end.

Finally, the plate was given a realistic thickness in y-direction. This was done by implementing Equation (2.4) into MATLAB to find the desired values. Drawing a spline between the points in the STAR-CCM+ CAD tool was also done in this case. The semi 2-D fish geometry is shown in Figure 4.3 (a) for the whole domain, and in (b) zoomed in at the fish itself.

(a) The whole computational domain.

(b) Zoomed in at the thin carangiform plate in its initial position.

Figure 4.2: Geometry of carangiform plate. Referring to Figure 3.3 (b), $b = 4$ m, $h = 2$ m and $L = 0.7$ m.
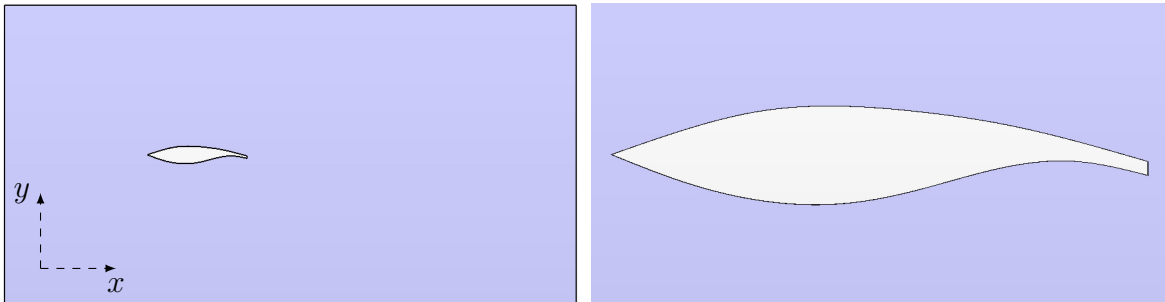
(a) The whole computational domain.

(b) Zoomed in at the carangiform semi 2-D fish.

Figure 4.3: Geometry of semi 2-D fish. Referring to Figure 3.3 (c), $b = 4$ m, $h = 2$ m and $L = 0.7$ m.

4.1.2 Meshing

Meshing is usually the second step during preprocessing. The geometry is divided into cells where the discretization discussed in Section 2.2.3 is done for each cell. STAR-CCM+ is equipped with a semiautomatic meshing tool allowing the user only to focus on the boundaries. When appropriate mesh controls are given for the crucial parts of the geometry (*i.e.* close to the walls and areas of interest), the mesh is automatically generated.

For the flat plate, the mesh was chosen to have twenty prism layers where each layer has a

thickness of 1.5 times the previous one. The total prism layer thickness was set to 0.015 m = 1.5 cm. These characteristics were set to be a surface control at the plate. The further away from the plate, the bigger the cells. The base size, *i.e.* the size of the biggest cells in the domain, was set to 0.1 m. No special attention was given to the wake in this case, as only the behaviour of the boundary layer was of interest, which the flow far behind the plate does not affect. Figure 4.4 (a)-(d) presents the mesh for the fixed flat plate.

The mesh for the carangiform thin plate is done in the exact same way and is shown in Figure 4.5 (a)-(d). No wake refinement is needed here either as we are only interested in the motion and grid deformation close to the plate, not the flow.

Finally, for the semi 2-D fish, these prism layer conditions were not enough any more. The prism layer thickness is extended to 4 cm with a total of 50 prism layers. Each layer does not have a thickness of 1.5 times the previous one anymore, but only 1.1 time. The base size is however still the same. These adjustments were done as the flow around the fish will be in focus from now on. A wake refinement was added behind the fish in order to calculate the reversed Kármán vortex street properly. The final mesh is shown in Figure 4.6 (a)-(d).
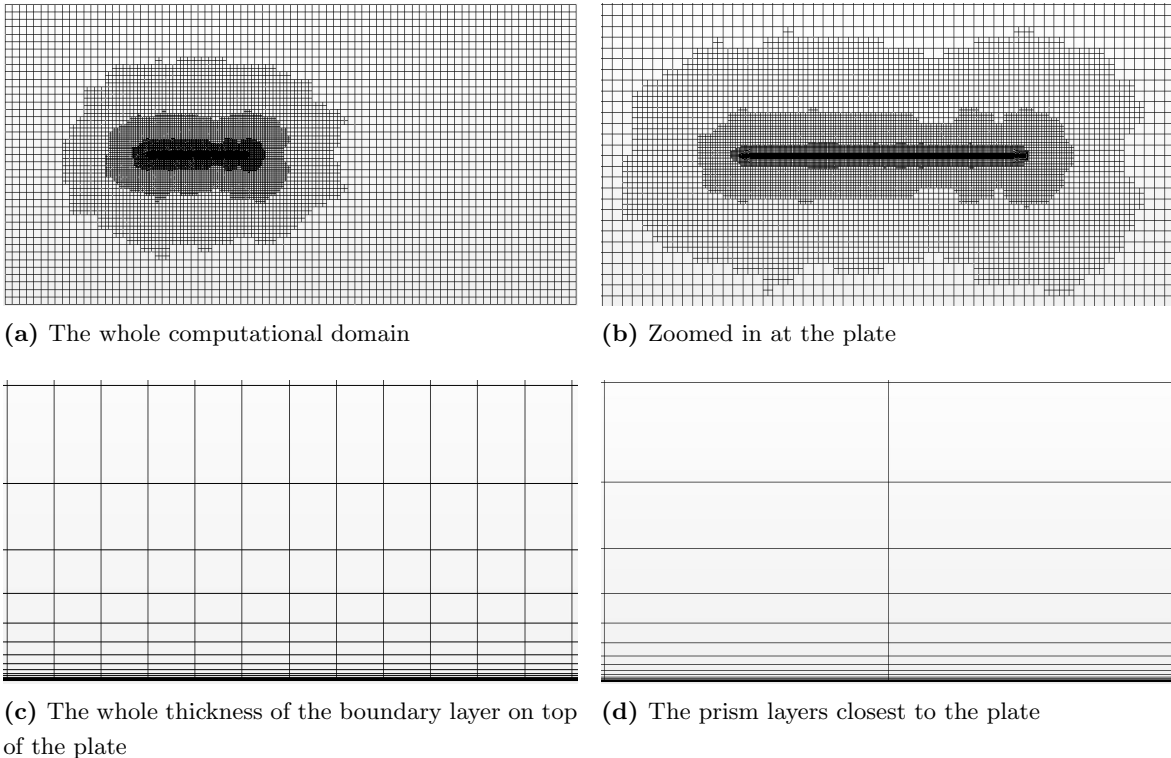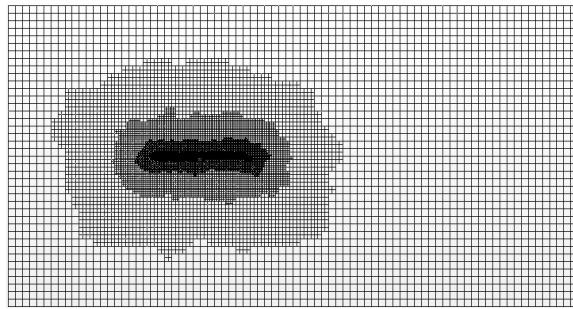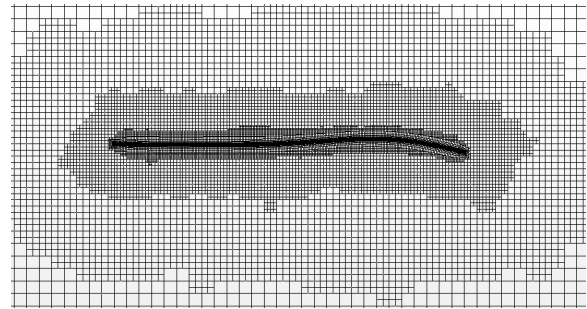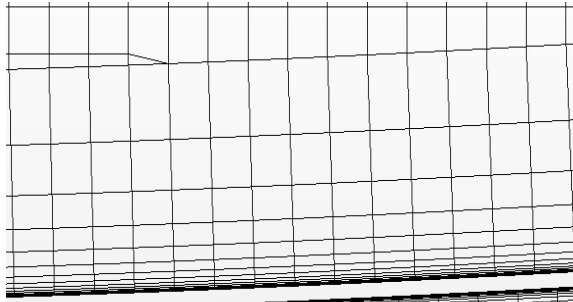

(a) The whole computational domain

(b) Zoomed in at the plate

(c) The whole thickness of the boundary layer on top of the plate

(d) The prism layers closest to the plate

Figure 4.4: Mesh for fixed flat plate with base size 0.1 m and 20 prism layers with a total thickness of 1.5 cm.
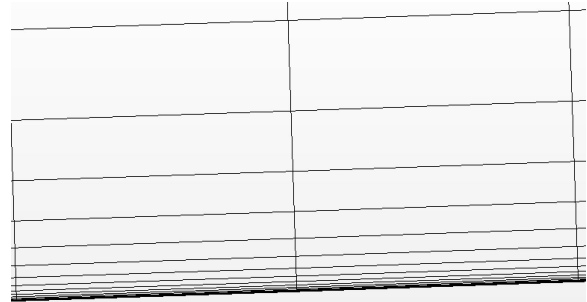
(a) The whole computational domain

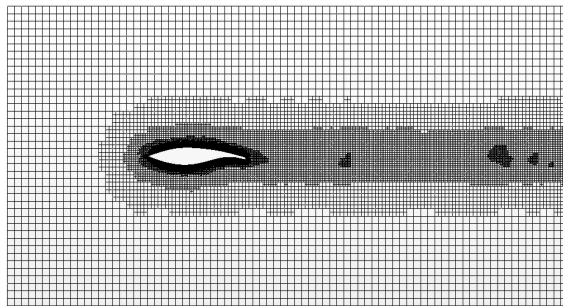**(b)** Zoomed in at the carangiform plate
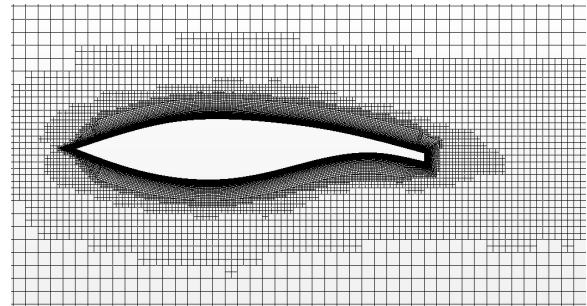
(c) The whole prism layer thickness

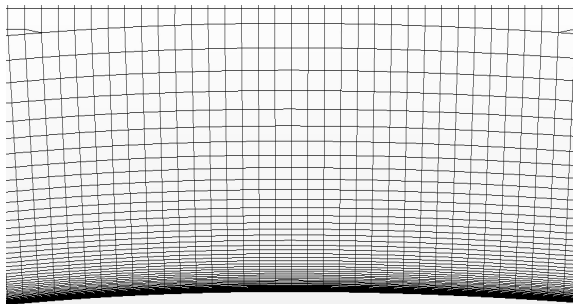**(d)** The prism layers closest to the carangiform plate

Figure 4.5: Mesh for carangiform thin plate with base size 0.1 m, 20 prism layers in a total thickness of 1.5 cm.

(a) The whole computational domain

(b) Zoomed in at the carangiform fish

(c) The whole prism layer thickness

(d) The prism layers closest to the fish wall

Figure 4.6: Mesh for semi 2-D fish with base size 0.1 m and 50 prism layers in a total thickness of 4 cm. Wake refinement is included to get more detailed calculations on the flow behind the fish.

4.1.3 Physics Models

The third step in preprocessing is setting up the physics models. They define all the environmental conditions and values within the model domain. The user interface for this part in STAR-CCM+ is shown in Figure 4.7 (a). There are six different physics that need to be set; space, time, material, flow, equation of state and viscous regime.

Space

The primary function of the space models is to provide methods for computing and accessing mesh metrics. There are four such models available in STAR-CCM+:

- The axisymmetric model is designed to work on two-dimensional axisymmetric meshes.

- The shell three-dimensional model is required when modeling heat conduction within a solid shell or modeling fluid films.

- The two-dimensional model is designed to work on two-dimensional meshes.

- The three-dimensional model is designed to work on three-dimensional meshes in cases where all spatial directions are relevant.

This project is working with a 2-D slice of a 3-D model, so one should believe that the 2-D model would satisfy our requirements. However, as bad results were obtained in the specialization project [1] when using 2-D space, the 3-D model is chosen. Only one cell is used in the third dimension to imitate the 2-D slice of a 3-D case, and to reduce time costs and complexity. The FVM discussed in Section 2.2.3 is used for the space discretization in STAR-CCM+.

Time

Time models in STAR-CCM+ provide solvers that control the iteration and/or unsteady time-stepping.

- Steady is used for all steady-state calculations, *i.e.* only spatial derivatives are discretized.

- Implicit unsteady advance in time in a marching manner updating the solution at each time-step using an algorithm called SIMPLE.

- Explicit unsteady is updating the solution at each time-step, but only compatible with inviscid and laminar viscous regime models within the coupled energy model.

- Harmonic Balance is transforming unsteady time-periodic problems into steady-state problems using Fourier series for example for axial flow turbomachinery, centrifugal machines or helicopter rotors.

- PISO unsteady is an alternative for the SIMPLE algorithm. It does not have inner iterations, so the number of iterations is the same as number of time steps. It should only be used for cases with small time steps (*e.g.* less than $\Delta t = 1 \cdot 10^{-6}$ s).

For the laminar case of constant flow over a flat plate the steady model could be used as it does not change with time. However, to be able to see time steps (and not only iterations) the implicit unsteady model is chosen. This is also the natural time model for all the other simulations, as we are working with turbulent viscous flow with relatively big time steps.

Material

The material model is responsible for managing the material being simulated in the continuum. There are three general types of material models available in STAR-CCM+:

- Single-component models are modelling pure substances in their fundamental states, including both liquids and gases. For those fluids numerical approximations to the solution of the governing fluid flow equations are obtained.

- Multi-component models are single-phase models for simulating fully miscible mixtures of two or more pure substances in the same phase. These models can be either reacting of non-reacting.

- Multiphase is simulating two or more immersible phases, where each phase is composed of a pure gas or liquid substance.

As water is the material of interest, liquid is chosen as the defined single-component material. The properties can be set later to match the most important groups of non-dimensional variables within the flow field. The physics model interface now looks like Figure 4.7(b).
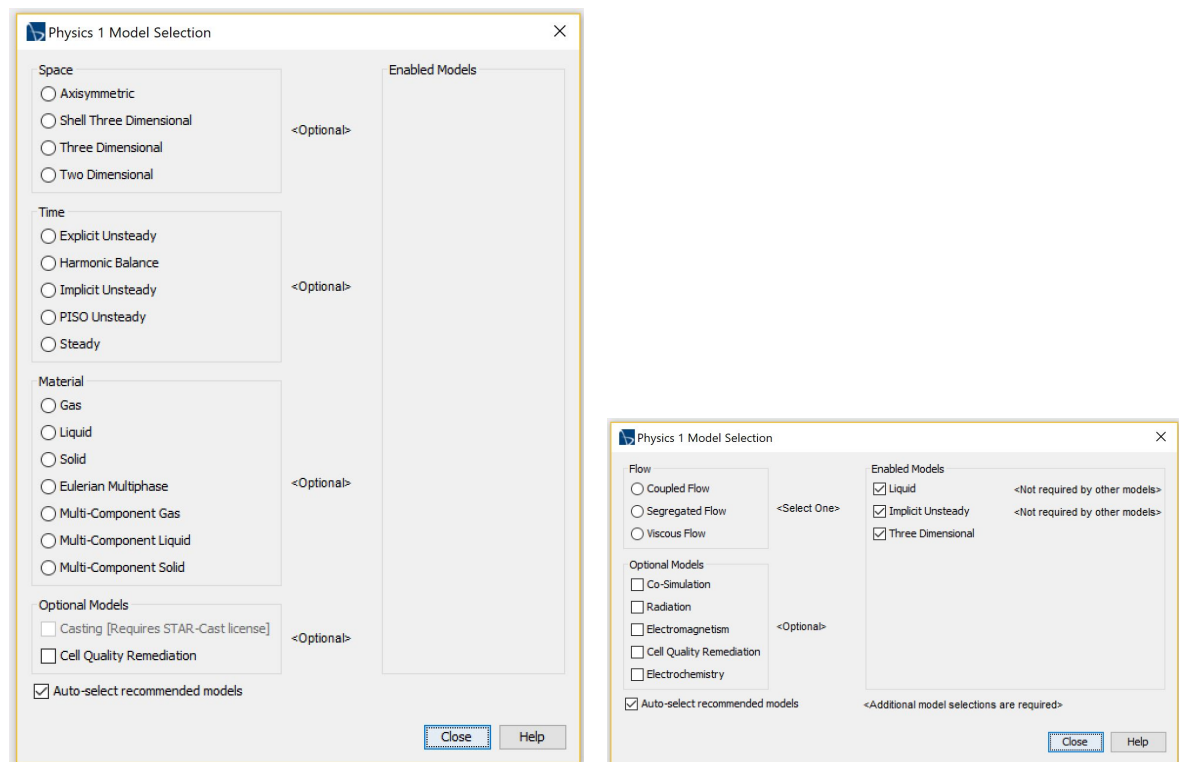
(a) Initial physics model selection.

(b) Physics model selection after choosing space, time and material.

Figure 4.7: User interface when choosing the physics models for the simulation in STAR-CCM+ part 1.

Flow

There are three flow models in STAR-CCM+:

- Coupled flow solves the conservation equations for mass and momentum simultaneously using a time- (or pseudo-time-) marching approach. The preconditioned form of the governing equations used by the coupled flow model makes it suitable for solving incompressible and isothermal flows.

- Segregated flow solves the flow equations (one for each component of velocity, and one for pressure) in a segregated, or uncoupled, manner. The linkage between the momentum and continuity equations is achieved with a predictor-corrector approach.

- Viscous flow allows the simulation of things such as paints, adhesives, foodstuffs and blood which behaves both as a solid (elastic) and a fluid (highly viscous).

The working flow is assumed to be incompressible which makes the pressure and velocity field the two variables to solve for. Segregated flow is chosen in which the pressure and velocity field will be found separately by solving the flow field governing equations numerically. After the flow model is chosen the interface looks like in Figure 4.8 (a).

Equation of State

In physics and thermodynamics an equation of state is a thermodynamic equation relating state variables which describe the state of matter under a given set of physical conditions. These can be for example pressure, volume, temperature or internal energy. STAR-CCM+ provides four equations of state:

- Constant density.

- IAPWS-IF97 (water, recommended for industrial use (primarily the steam power industry) for the calculation of thermodynamic properties of ordinary water in its fluid phases, including vapor-liquid equilibrium).

- Polynomial density.

- User defined state.

The flow of interest is in the subsonic regime. Variation of density with respect to the pressure can therefore be neglected. As a result of this assumption one can define the working fluid to be incompressible and the constant density option is chosen as the equation of state.

Viscous Regime

The viscous regime decides if the simulation is going to be solved for inviscid, laminar or turbulent flow. A laminar viscous regime was first chosen for the fixed flat plate. When the flat plate starts moving the boundary layer might turn turbulent. Different turbulent models were therefore tested with a turbulent boundary layer over flat plate to see which turbulence model was best suited for boundary layer treatment. In this case, the turbulent viscous regime was chosen. Several different options of turbulence models are available, as

shown in Figure 4.8 (b). Note that DNS is not an option in STAR-CCM+, but DES, LES and RANS all have several model choices.
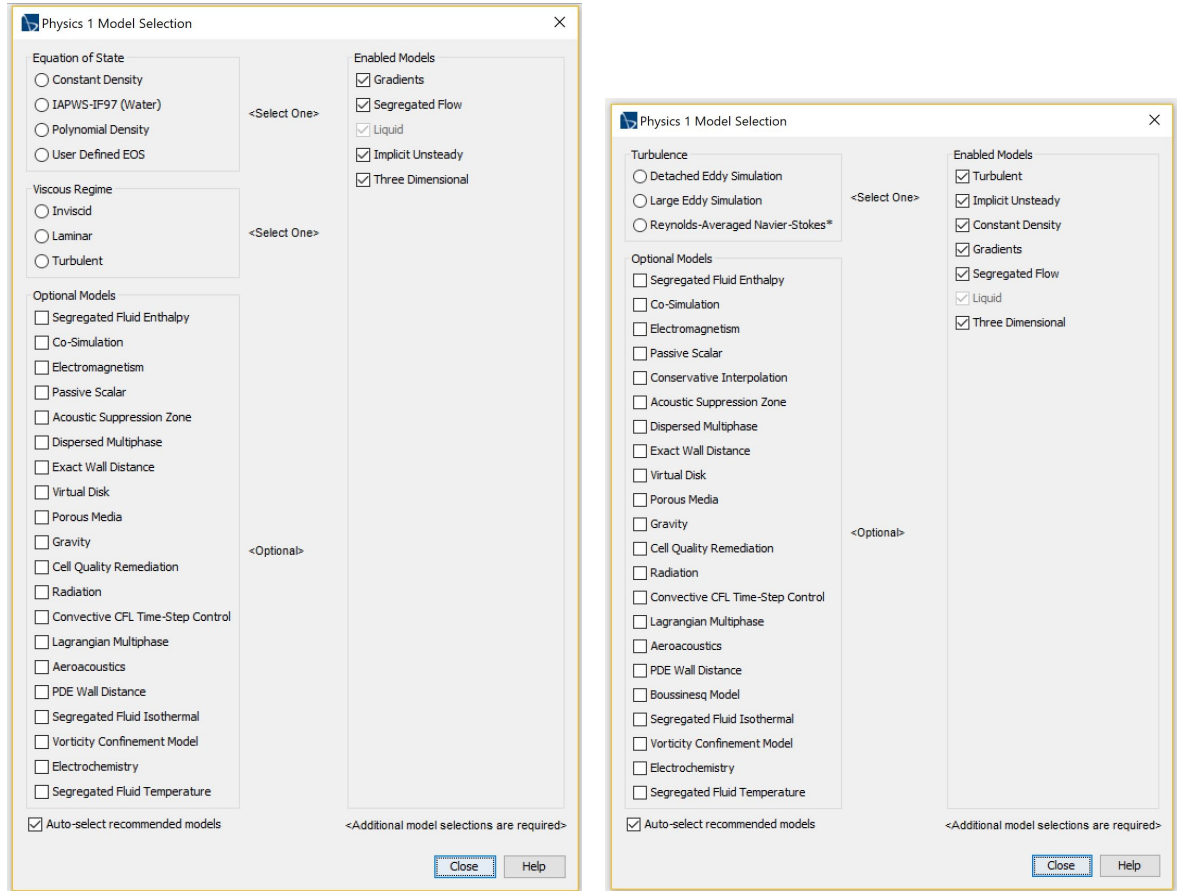
(a) Physics model selection after choosing a flow model.

(b) Physics model selection after choosing the viscous regime.

Figure 4.8: User interface when choosing the physics models for the simulation in STAR-CCM+ part 2.

All the LES and DES models are listed in Table 4.1. All the RANS models are listed in Table 4.2. With over 20 turbulence models to choose from, it is not easy to pick *the right one*, nor the least the most fitting one. It might, however, be a good idea to exclude as many as possible. As LES models are best suited in cases where there are larger three-dimensional unsteady turbulent motions, is will not be suited for the problem of interest. The turbulence in the flow of interest mostly lies in the boundary layer and wake, where RANS would have to step in anyways. As DES also uses the characteristics of LES models all the models in Table 4.1 are excluded, and will not be investigated further.

Table 4.1: Detached eddy simulation (DES) and large eddy simulation (LES) models available in STAR-CCM+.

DES	LES
EB k-ε detached eddy	Dynamic smagorinsky subgrid scale
SST meter k-ω detached eddy	smagorinsky subgrid
Spaltar-Almaras detached eddy	WALE subgrid scale

Table 4.2: Reynolds-Averaged Navier Stokes turbulence models available in STAR-CCM+; K-Epsilon (k-ε), K-Omega (k-ω), Reynolds Stress (RS) and Spalart-Allmaras (S-A) models. P is short for pressure. *Pre-selected models in STAR-CCM+.

k-ε	k-ω	**RS**	**S-A**
AKN low-Re	SST Menter*	Elliptic blending	High-Re
Elliptic blending (EB)	Standard (Wilcox)	Linear P strain	standard
Lag EB		Linear P strain two-Layer	
Realizable		Quadratic P strain	
Realizable two-layer*			
Standard			
Standard low-Re			
Standard two-layer			
V2F			

Reynolds Stress models are used for computing cyclone flows, swirling flows in combustors, rotating flow passages, and the stress-induced secondary flows in ducts, as they account for the effects of streamline curvature, swirl, rotation, and rapid changes in strain rate in a more physical manner than that by one-equation or two-equation models. They will therefore be excluded. The same goes for Spalart-Allmaras models as they have clear limitations because they are one-equation models, and are intended for aerodynamic flows. Thus, the remaining categories of turbulence models are the k-ε and k-ω models.

A small description for each of the k-ε and k-ω models are presented in Appendix C. Four k-ε (Lag EB, Realizable Two-Layer, Standard Two-Layer and V2F) and the two k-ω models were decided to be investigated for the turbulent boundary layer over a flat plate. This was based on which ones seemed most fitting for the problem.

4.1.4   Moving Grid

Motion is defined as the change in location of a body relative to a particular frame of reference. STAR-CCM+ distinguishes between three broad categories:

- *Mesh displacement in real time* is actual displacement of mesh vertices in real time and are used for transient analysis.

- *Moving reference frame in steady-state* gives a solution that represents the time-averaged behaviour of the flow, rather than the time-accurate behaviour.

- *Harmonic balance flutter* is used in simulations that involve the harmonic balance method with blade vibration.

Most marine and offshore analyses are transient by nature and require that mesh vertices are displaced in real-time. There are four real-time models to choose from:

- *Rigid motion of the whole mesh* is suitable for a single body moving in an infinite environment and a flat free surface.

- *Mesh morphing* keeps the grid topology and moves the internal vertices according to the boundary motion.

- *Embedded (sliding) interfaces* is following the body movement, the whole mesh is translated while the region around the body is rotated using a sliding grid approach.

- *Overset mesh* has one background grid fixed to the environment and one overlapping grid is attached to each moving body.

Both overset mesh and morphing mesh were options for this thesis. As the computational domain is relatively small and semi 2-D, the mesh morphing tool where selected. To set motion to the plate, the motion needed to be defined as a field function and assigned to the plate. Equation (2.1) for BCF motion with Equation (2.2) for the amplitude gives

$$h(x, t) = (a_1 + a_2 x + a_3 x^2) \sin(\omega t - kx) \tag{4.1}$$

for the motion of a carangiform fish. This equation represents the midline position in space. STAR-CCM+, however, requires the motion based on its velocity as input. Equation (4.1) is therefore derived with respect to time to get the velocity equation for the motion

$$h'(x, t) = \omega(a_1 + a_2 x + a_3 x^2) \cos(\omega t - kx). \tag{4.2}$$

The parameters inserted into this equation are presented in Table 4.3. They where chosen in a way to make the carangiform motion be as similar as possible to a farmed Atlantic salmon. These values give a swimming period of $T = 1/f = 0.67$ s. Equation (4.1) was implemented into MATLAB and plotted for different values of t for one period as shown in Figure 4.9. This was done to be able to verify that the motion in STAR-CCM+ was as expected.

Table 4.3: Parameters needed for the inserted motion equation (4.2) in STAR-CCM+.

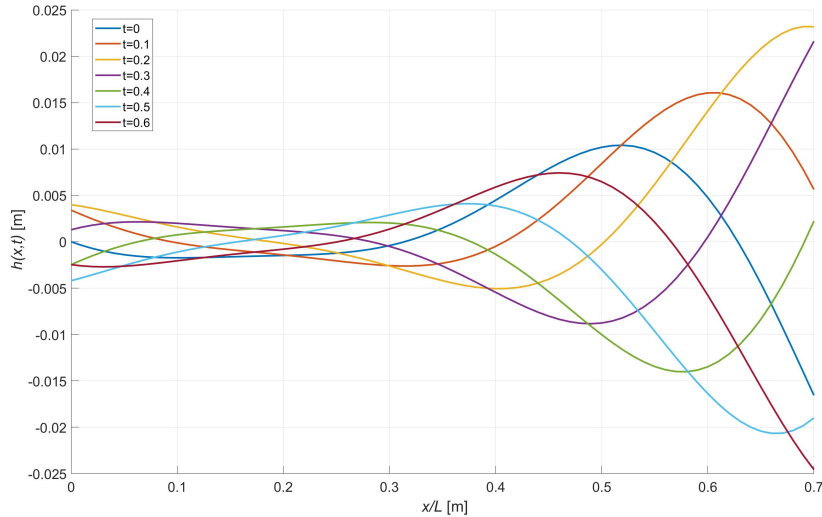| Condition	Notation	Unit	Value
Fish length	L	[m]	0.7
Wave number	k	[m^{-1}]	$7/L$
Tail beat frequency	f	[Hz]	1.5
Tail beat frequency	ω	[s^{-1}]	$2\pi f$
First quadratic coefficient	a_1	[–]	$0.004fL$
Second quadratic coefficient	a_2	[–]	$-0.02f$
Third quadratic coefficient	a_3	[–]	$0.04f/L$

Figure 4.9: Midline position of carangiform thin plate at different time steps.

4.1.5 Initial and Boundary Conditions

The final step in preprocessing is to set the initial and boundary conditions. STAR-CCM+ provides 8 different boundary conditions; mass flow inlet, stagnation inlet, velocity inlet, overset mesh, symmetry plane, wall (slip or no-slip), outlet and pressure outlet.

The flow is initially not bounded by any walls, and the right and left side boundary (Figure 2.6) is therefore set to symmetry walls. This means that what happens on the inside of this boundary also happens on the outside. The flow exits the domain through the outlet face which is set to a pressure outlet. The flow enters the domain from the inlet face with constant and uniform velocity, *i.e.* a velocity inlet. Later on the boundary conditions on the right and left sides were changed to walls, where the distance from the fish to the walls varied. The initial conditions that need to be set are only the constant incoming velocity and outlet pressure, which is set to 0.4 m/s and the atmospheric pressure (*i.e.* zero gauge pressure), respectively. The final domain sketch after all the preprocessing is shown in Figure 4.10.
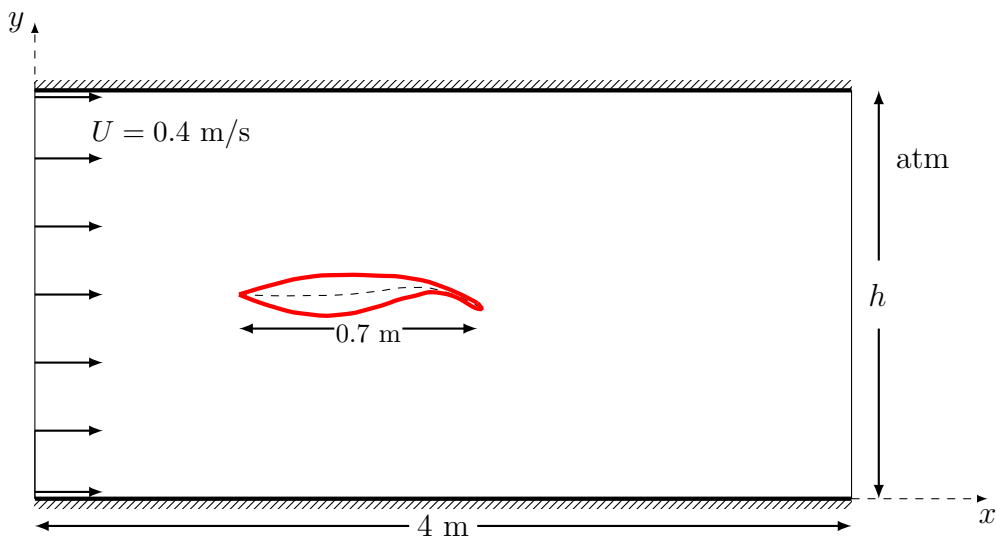

Figure 4.10: Domain sketch of semi 2-D fish between two walls with constant incoming flow $U = 0.4$ m/s, fish length $L = 0.7$ m, water column width $b = 4$ m and variable height h.

35

4.2 Simulating

When all the preprocessing is in order, it is time to run the simulation. The simulation is run at least until the solution is stable, *i.e.* the residuals are nice and flat. The residuals show the residual difference either between the defined output and the last iteration of the algorithm, or simply the last iteration of the algorithm and its penultimate iteration. They are important because they tell how well the simulation has converged to an acceptable approximation of real life flow. The Courant number is checked to see if the Δt is small enough, and the y^+ is checked for turbulent cases to check if the Δx is small enough. A summary of the physical condition values given and the expected outcome are presented in Table 4.4 for the flat plate simulations. Note that the flow velocity is increased in the turbulent case to obtain a fully turbulent boundary layer. For the moving grid simulations, a summary of the input values are presented in Table 4.5.

Table 4.4: Physical conditions for laminar and turbulent flow a over fixed flat plate.

Condition	Notation	Unit	Laminar	Turbulent
Fluid density	ρ	[kg/m^3]	997.56	997.56
Dynamic viscosity	μ	[Pa·s]	$8.887 \cdot 10^{-4}$	$8.887 \cdot 10^{-4}$
Reference pressure	p	[Pa]	0	0
Plate length	L	[m]	0.7	0.7
Flow velocity	U	[m/s]	0.4	1.5
Reynolds number$\|_{x=L}$	Re	[–]	$3.1 \cdot 10^5$	$1.2 \cdot 10^6$
Boundary layer thickness$\|_{x=L}$	δ	[m]	0.00629	0.015–0.016
Skin friction coefficient$\|_{x=L}$	C_f	[–]	0.00119	0.0036–0.0037

Table 4.5: Physical conditions for moving grid simulations.

Condition	Notation	Unit	Value
Fluid density	ρ	[kg/m^3]	997.56
Dynamic viscosity	μ	[Pa·s]	$8.887 \cdot 10^{-4}$
Reference pressure	p	[Pa]	0
Plate length	L	[m]	0.7
Flow velocity	U	[m/s]	0.4
Reynolds number$\|_{x=L}$	Re	[–]	$3.1 \cdot 10^5$
Wake width	H	[m]	0.07
Strouhal number$\|_{x=L}$	St	[–]	0.19
Wave number$\|_{x=L}$	k	[–]	10
First amplitude coefficient	a_1	[–]	0.0042
Second amplitude coefficient	a_2	[–]	-0.03
Third amplitude coefficient	a_3	[–]	0.086
Tail beat frequency	ω	[s^{-1}]	9.425
Tail beat frequency	f	[Hz]	1.5
Period	T	[s]	0.67

4.3 Postprocessing

Visualizing and analyzing the results after a simulation is called postprocessing. This is really the main goal of a simulation; to get results, and to be able to read them. Different choices for postprocessing such as reports, monitors, plots and scenes are available in STAR-CCM+.

Reports create the data of the results obtained during the simulation. This includes forces, moments, coefficients, maximal and minimal values, fluxes, areas etc. They are created in the STAR-CCM+ interface and set to the parts of interest. The result for the last time step appears in the output window.

A monitor can be created from a report as an alternative when more values are needed. The monitor represents an output table of the results for each time step. It can either be exported as a .csv file for plotting and analyzing in *e.g.* MATLAB, or it can be plotted directly in STAR-CCM+.

Plots are presenting the results in graphs. Plots from monitors are always as a function of time. However, it is possible to plot as a function of for example x-position for the last time step by creating an XY-plot directly. A report or monitor is not needed in this case. An XY-plot might be handy for example when comparing solutions from the simulation with analytical solutions defined as a field function.

Creating scenes makes it possible to visualize different aspects of the simulation, including velocity, pressure, Courant number, wall y^+ value, vortices etc. Scalar and vector scenes are typical scenes used to show results. Different choices of color bars, field size etc. makes it easy to distinguish the different variables.

It is important to keep in mind that no preprocessing can be 100 % finished without doing both simulating and postprocessing first. It takes several trial runs to figure out if the conditions that are set really are suitable in the working case. Mesh generating, initial conditions and the viscous regime have been changed again and again to find reasonable results, which again needs to be found through postprocessing. The whole CFD methodology is a cyclic approach, in which preprocessing, simulating and postprocessing need to be done over and over, and all the steps have influence on each other.

5. Results

In this chapter the results will be presented for each subtask in the same order as discussed in Section 3.3. The boundary layer thickness and skin friction coefficient will be presented first. Further, the grid deformation will be presented, and the position of the plate with carangiform motion will be compared to the analytical solution. The results showing how fish affect their surrounding flow will lastly be disclosed. It was decided to test for a system with one fish as discussed before, but also do a quick simulation of the same system with three fish to see if the increase of fish density made any difference to the results. All discussion will be treated in Chapter 6.

5.1 Fixed Flat Plate

The aim of the flat plate simulations was to verify STAR-CCM+'s approximation of the boundary layer over a fixed smooth flat plate in constant parallel flow. The boundary layer is an important characteristic when looking at fish motion and their surrounding flow, and is a fundamental case supported by literature. The simulations were implemented with the values presented in Table 4.4, and compared to the analytical solutions for boundary layer thickness and skin friction coefficient summarized in Table 2.1. For the turbulent case, six different turbulence models were tested; the standard two-layer, realizable two-layer, V2F and lag EB k-ε models, and the standard Wilkox and SST Meter k-ω models.

5.1.1 Laminar Boundary Layer

Figure 5.1 presents the resulting scalar and vector velocity field for the laminar constant flow parallel to the flat smooth plate. No attention will be paid to the very beginning and very end of the plate, as there will be disturbances here due to the thickness of the plate (1 mm). Figure 5.1 (a) shows the velocity field for the whole computational domain, whereas (b) is zoomed closer to the right side of the plate, showing the boundary layer. Figure 5.1 (c) presents the velocity vectors around the mid part of the plate and (d) is zoomed in at the boundary layer at the right side of the plate. The vectors are shown for each vertex of the grid cells, which means that the vertical distance between them increases with 1.5 times the previous one. There is a total of 20 vectors in the vertical direction of the boundary layer, with a total height of 1.5 cm. It is observed that the vectors in one column represents the velocity profile in the boundary layer.

A plot comparing the STAR-CCM+ simulation with Blasius' equation for laminar boundary layer thickness δ is shown in Figure 5.2 (a). The same is done for the skin friction coefficient C_f in Figure 5.2 (b). The simulation was done both with a pointed front end and a flat front end of the plate. This was done to see if the pointed end had any significant effects on the flow disturbances even for a plate with only 1 mm thickness.
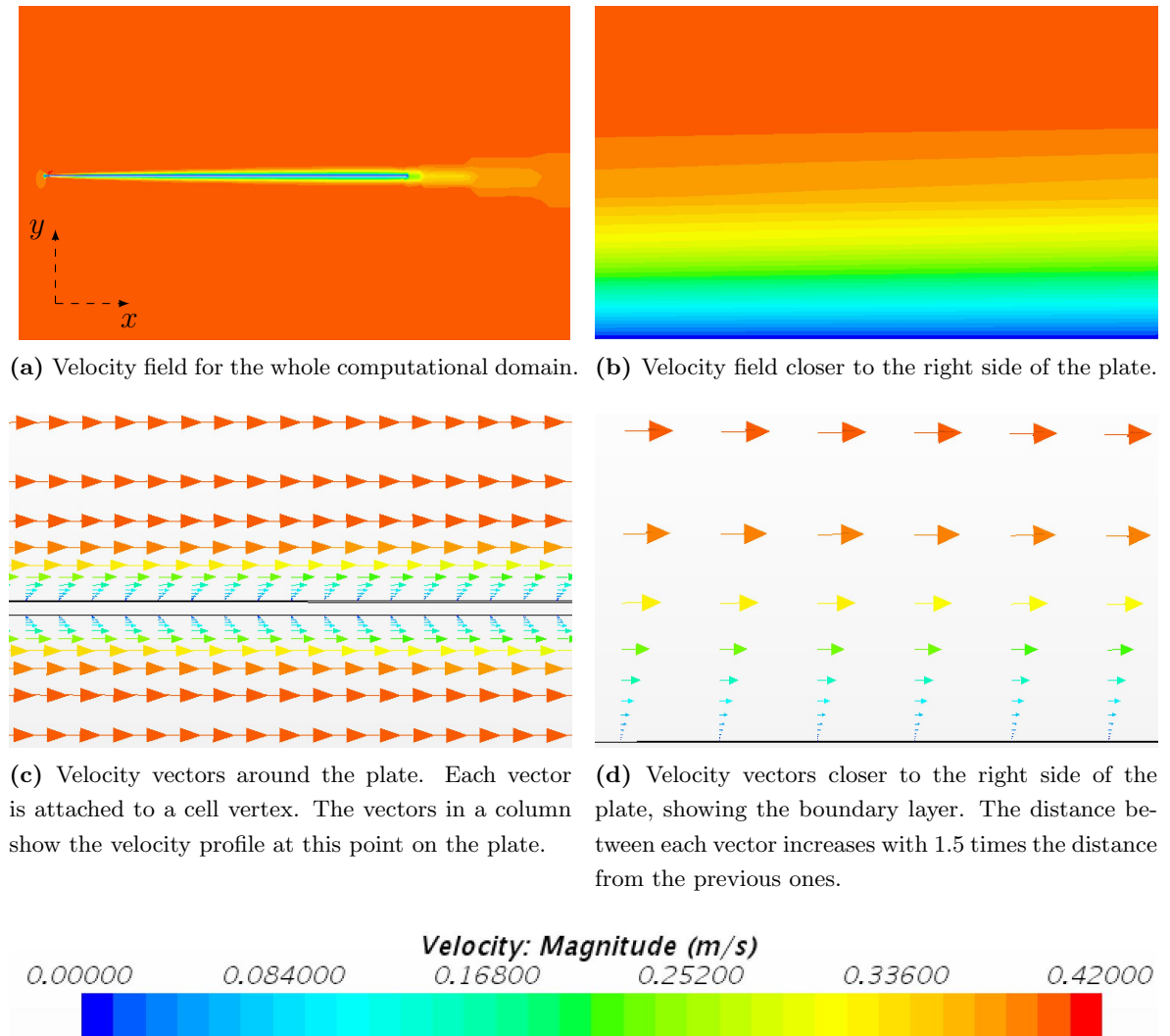
(a) Velocity field for the whole computational domain.

(b) Velocity field closer to the right side of the plate.

(c) Velocity vectors around the plate. Each vector is attached to a cell vertex. The vectors in a column show the velocity profile at this point on the plate.

(d) Velocity vectors closer to the right side of the plate, showing the boundary layer. The distance between each vector increases with 1.5 times the distance from the previous ones.

Figure 5.1: Flow velocity for laminar boundary layer over smooth flat plate in incoming parallel flow showing the whole domain and the boundary layer.
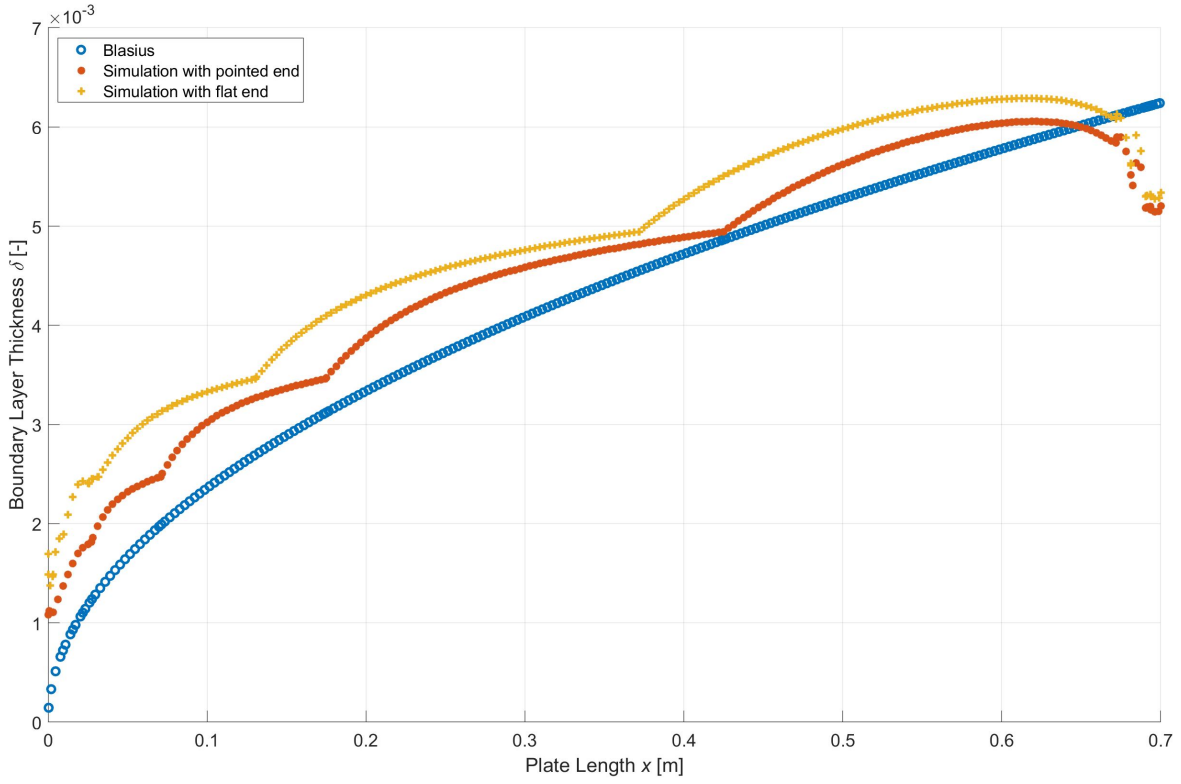
(a) Boundary layer thickness.
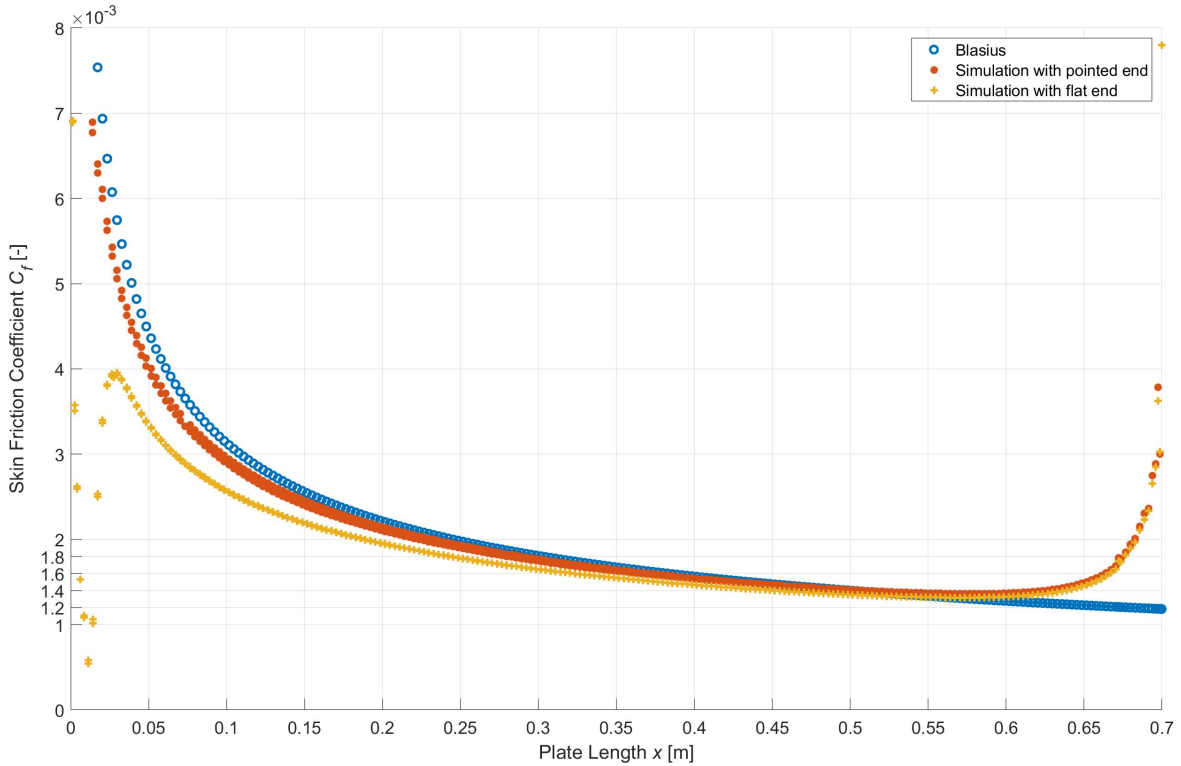
(b) Local skin friction coefficient.

Figure 5.2: Comparing STAR-CCM+ simulation with Blasius' equation for laminar boundary layer over smooth flat plate in incoming parallel flow. The simulation were done for two cases; one with a pointed front end and one with a flat one.

5.1.2 Turbulent Boundary Layer

The turbulent boundary layer over a flat plate was simulated with six different turbulence models. The standard two-layer, realizable two-layer, V2F and lag EB k-ε models, and the standard Wilkox and SST Meter k-ω models where chosen based on the discussion in Section 4.1.3. They were compared to each other and two analytical solutions for boundary layer thickness and skin friction coefficient summarized in Table 2.1. The incoming flow velocity was increased from 0.4 m/s to 1.5 m/s in order to obtain a fully turbulent boundary layer. The results are summarized in Figure 5.3.
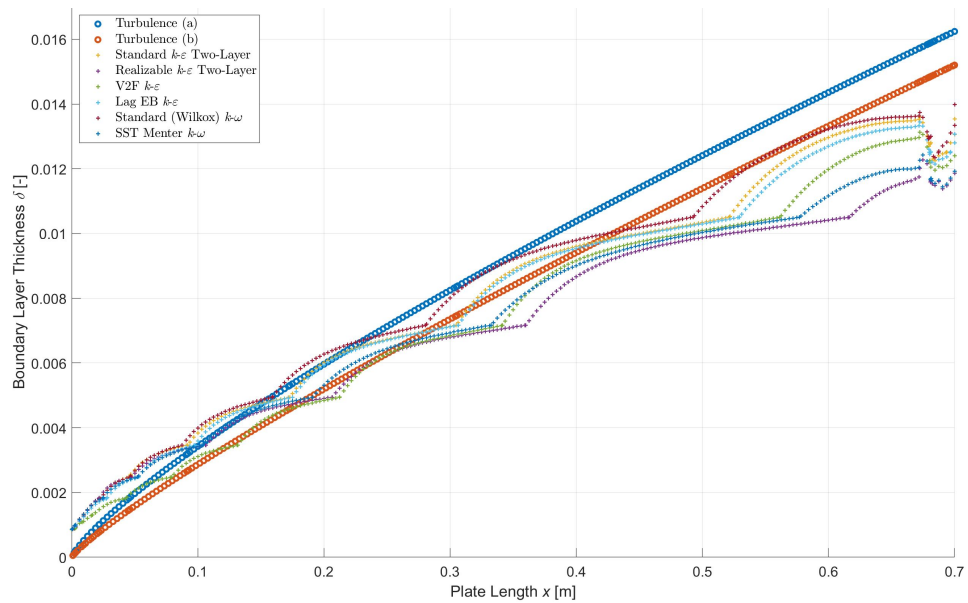
(a) Boundary layer thickness
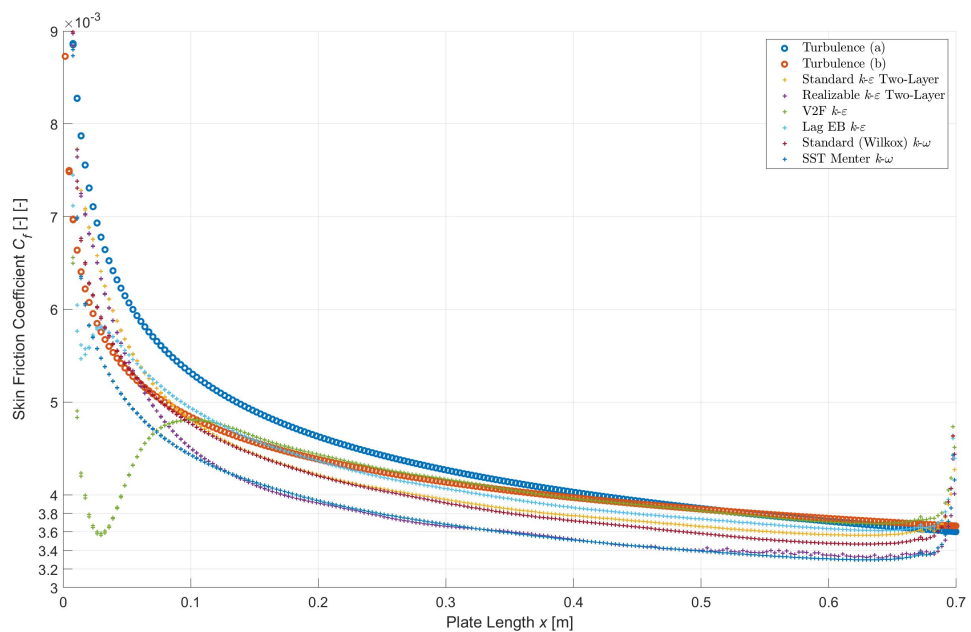
(b) Local skin friction coefficient

Figure 5.3: Comparing STAR-CCM+ simulation with analytical solutions for turbulent boundary layer over a smooth flat plate in incoming parallel flow for different turbulence models.

5.2 Carangiform Motion of Thin Plate

The aim of simulating the carangiform motion of a thin plate was to verify that the position of the midline in space was in accordance with the given function. It was also done to test the morphing mechanism, and to see that the grid around the plate moved according to the motion of the plate.

Figure 5.4 presents a comparison between the simulation and analytical solution of the position in space for carangiform motion of flat thin plate at different time steps. The lines of small circles represent the simulated solution whereas the solid lines represent the analytical solution. The time steps are chosen arbitrary throughout the simulation to show if the results are equally good throughout the simulation of 10 seconds.
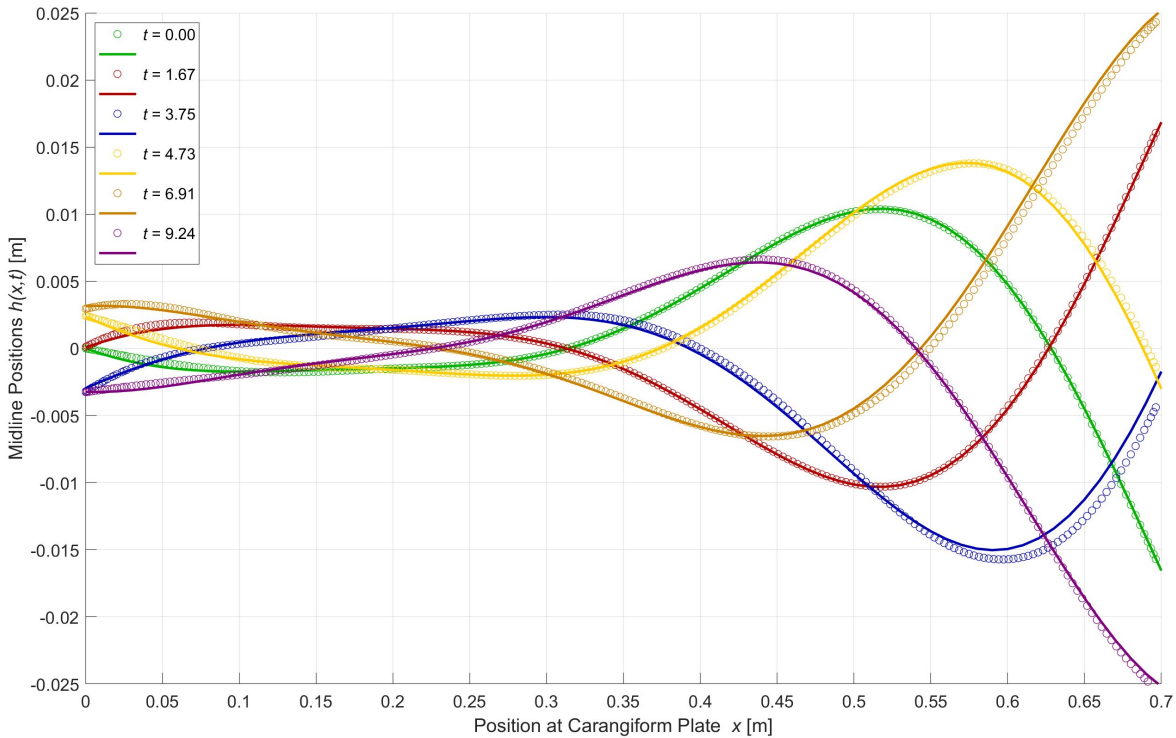
Figure 5.4: Comparing carangiform position from STAR-CCM+ simulation with analytical solutions found from Equation (2.1) and (2.2) at different time steps. The lines of circles represent the simulated solutions whereas the solid lines represent the analytical solutions. The time steps are chosen arbitrary throughout the simulation.

Looking at the morphing tool and the resulting grid deformation, figure 5.5 (a)-(f) presents the grid at the same time steps as in Figure 5.4. The deformation of the grid between the different time steps is observed, where the goal of the morphing tool is to follow the boundary motion of the plate in time without generating overlapping cells. The focus lies on the tail end of the plate as this is where the deformation is most significant.
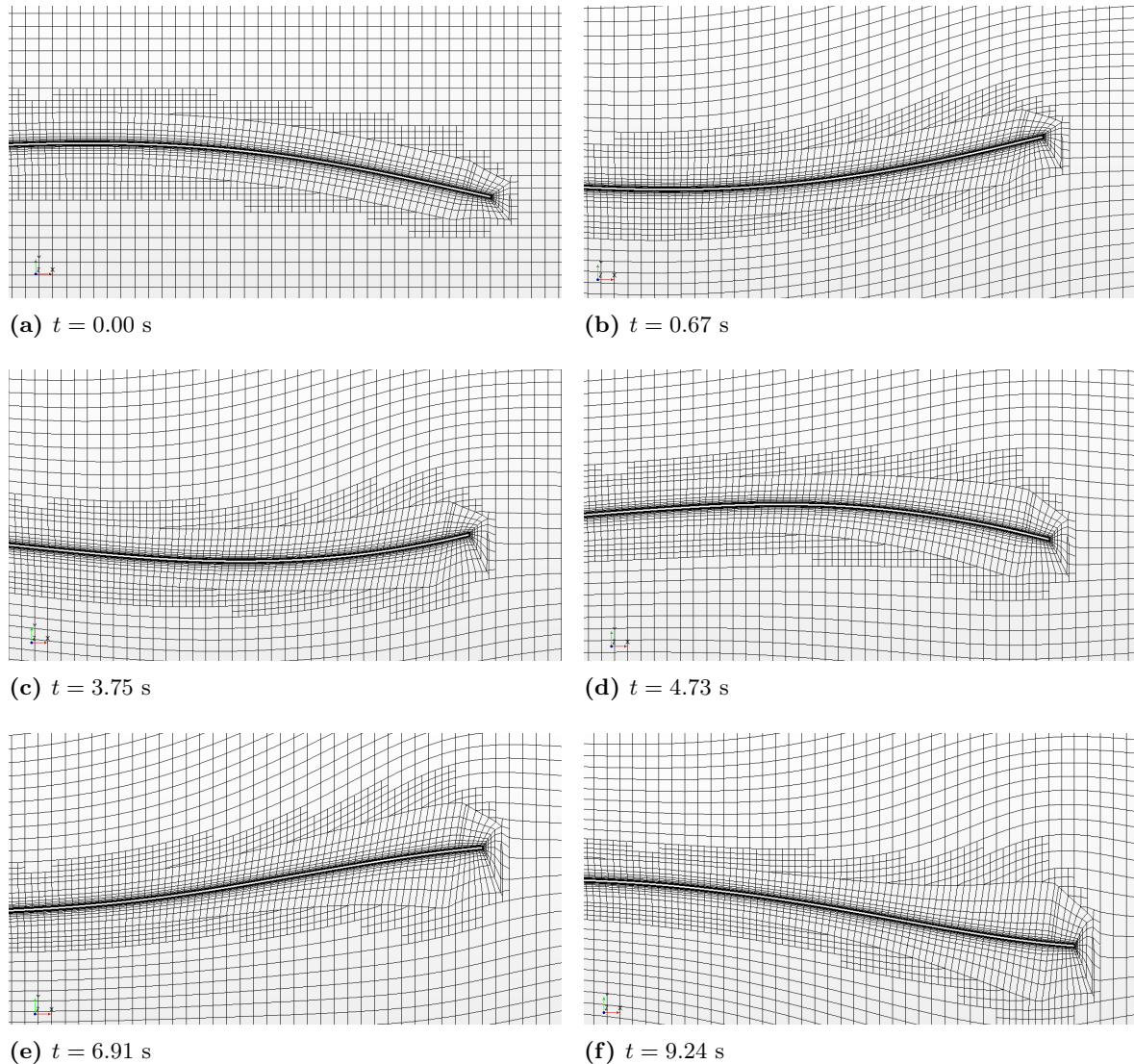
43

(a) $t = 0.00$ s

(b) $t = 0.67$ s

(c) $t = 3.75$ s

(d) $t = 4.73$ s

(e) $t = 6.91$ s

(f) $t = 9.24$ s

Figure 5.5: Grid deformation close to the back part of the thin plate at different time steps.
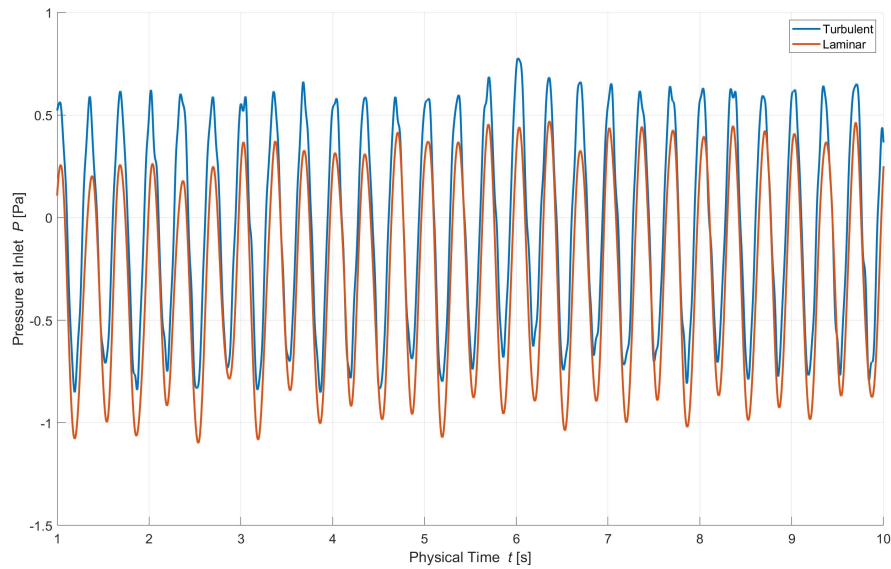
5.3   2-D Fish with Carangiform Motion

The aim of simulating a 2-D fish with carangiform motion was to be able to say something about how the flow in a closed fish farming cage is affected by the fish motion. The simulation was run with both laminar and turbulent viscous regime to see if this had any significant effects on the results. The standard k-ε two-layer model was used during all turbulent simulations.

5.3.1   Laminar vs. Turbulent

Plots looking at the differences between the laminar and turbulent simulation of a 2-D fish with carangiform motion are presented in Figure 5.6. The average pressure from the water on the fish during the simulation of 10 seconds is presented in Figure 5.6 (a). The average pressure at the inlet plane during the simulation of 10 seconds is presented in Figure 5.6 (b). Figure 5.6 (c) shows the total force acting on the fish in x-direction, *i.e.* the total drag force.
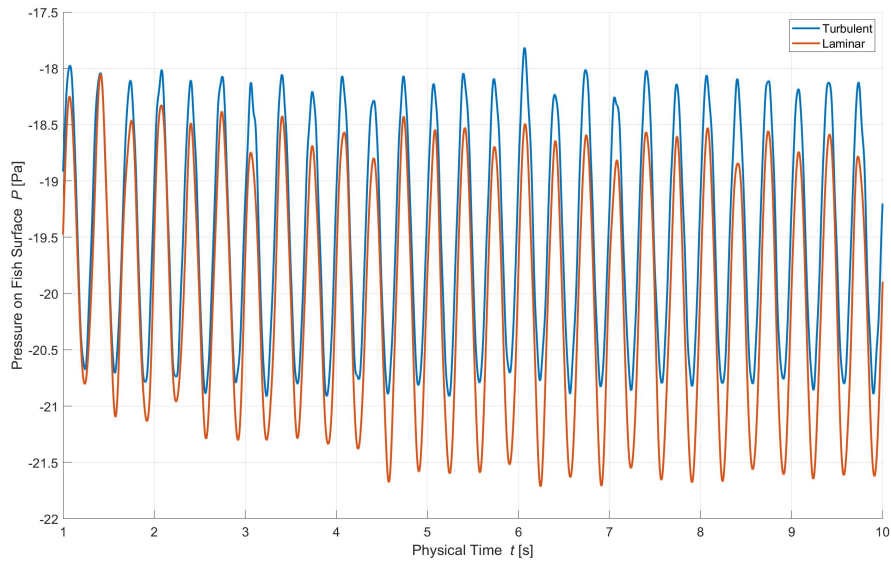
**(a)** Surface average of the pressure on the fish exerted by the water.

**(b)** Surface average of the pressure at the inlet plane exerted by the water.
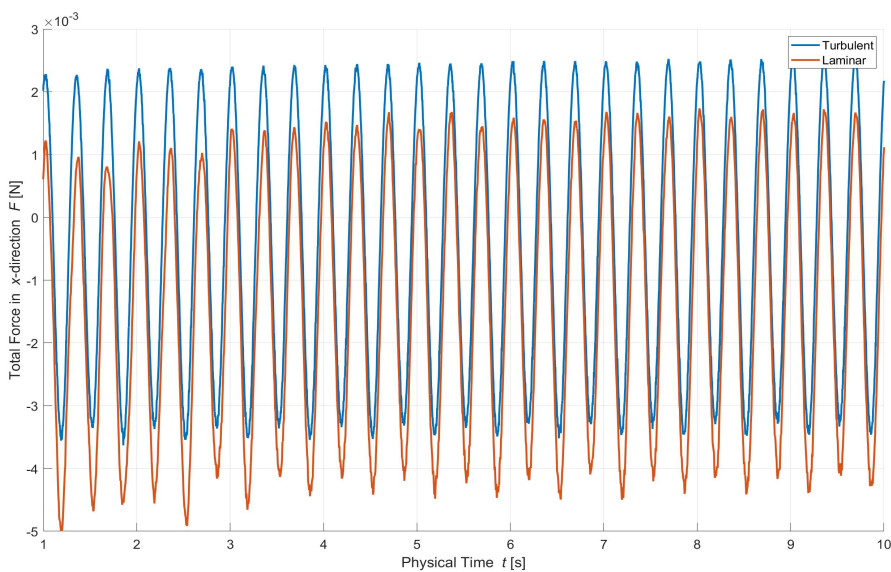
(c) Total force on the fish in x-direction exerted by the water.

Figure 5.6: Turbulent vs. laminar simulation of 2-D fish with carangiform motion.

45

Looking at a more visual result, the vorticity field in z-direction is shown for the laminar and turbulent simulation at time step $t = 10$ s in Figure 5.7. The red side of the color bar is going in clockwise direction whereas the blue side is going in counterclockwise direction.
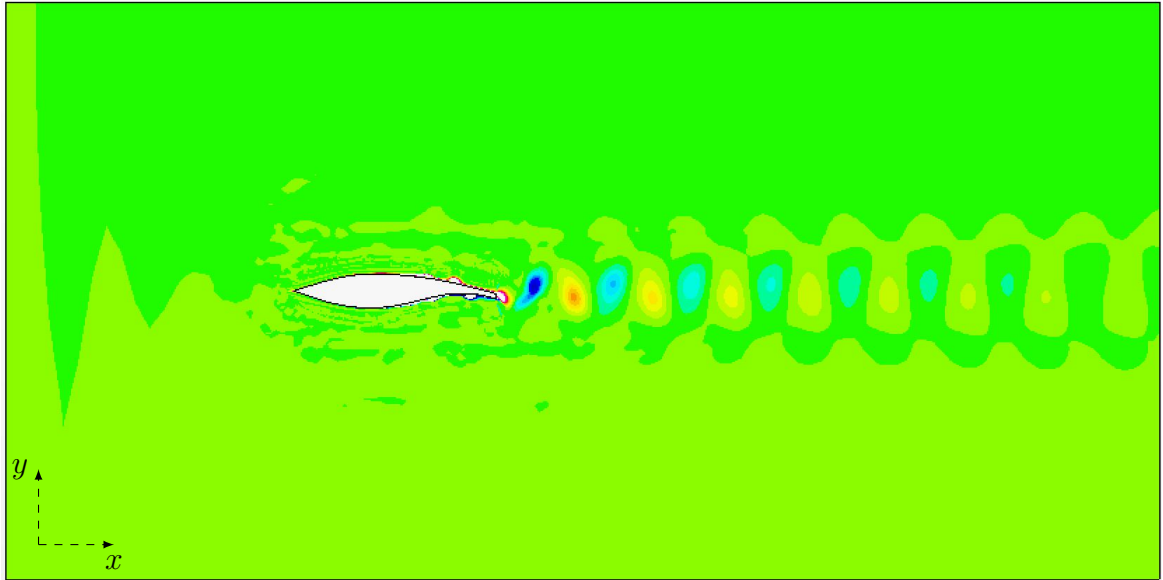
**(a)** Laminar solution.
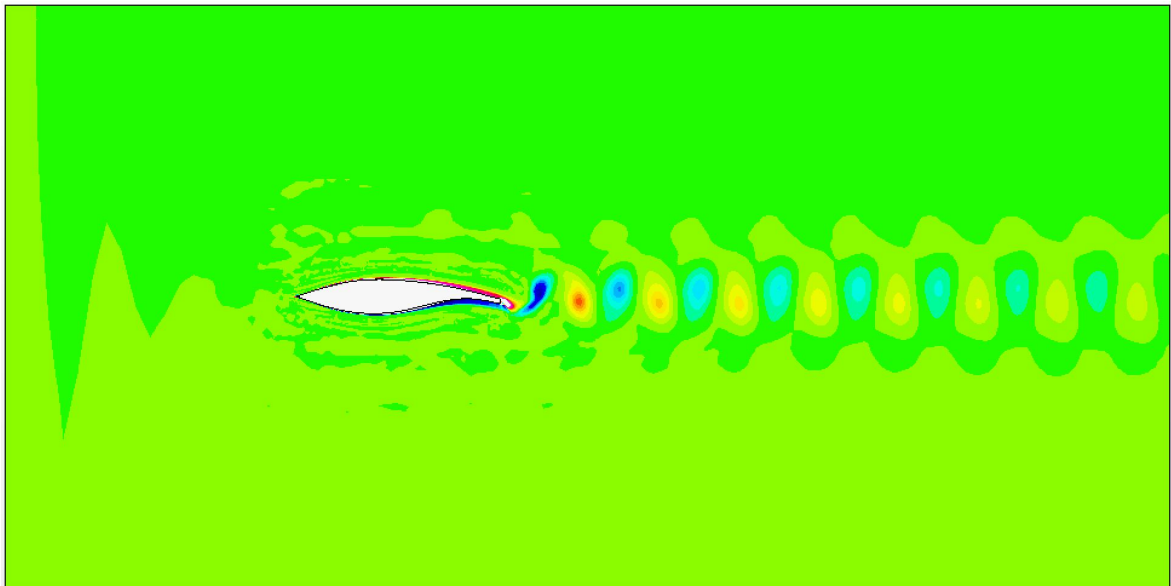
(b) Turbulent solution.

Figure 5.7: Vorticity field in z-direction for laminar and turbulent simulation of 2-D fish with carangiform motion at time step $t = 10$ s. Red indicates vortices in clockwise directeion whereas blue indicates vortices in counterclockwise direction.

5.3.2 Effects from Fish on the Surrounding Flow

Walls are added on the right and left sides of the fish, where the distance between them is decreased to see how this affects the pressure. The pressure is measured at the inlet plane, and the results are presented in Figure 5.8 (a). The pressure is also measured at the fish's surface to see if the results here are any different. This is presented in Figure 5.8 (b).
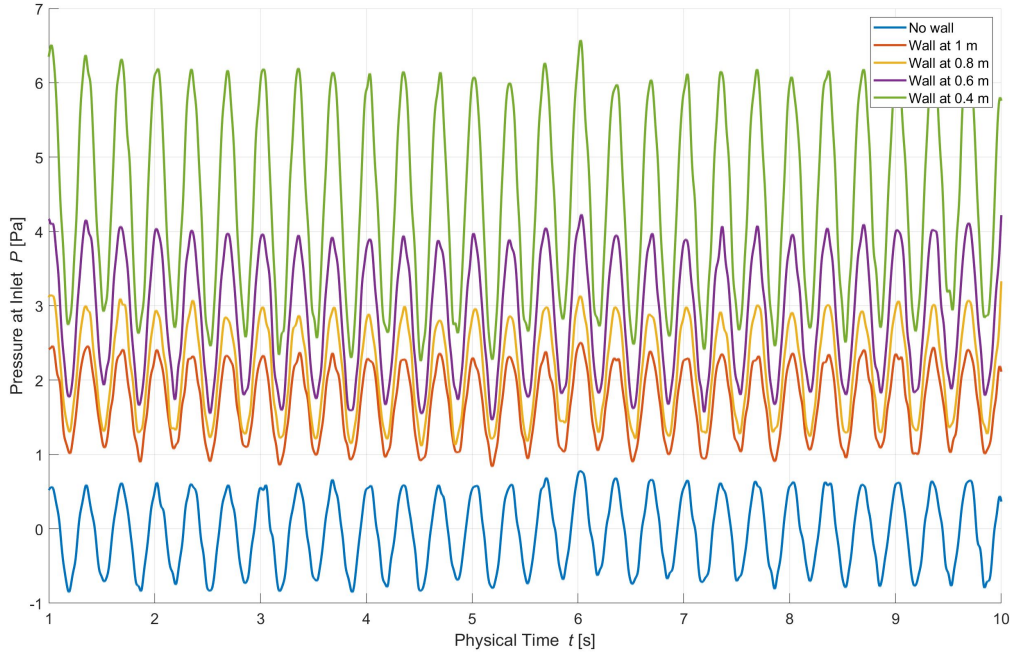
(a) Flow pressure average at inlet plane.
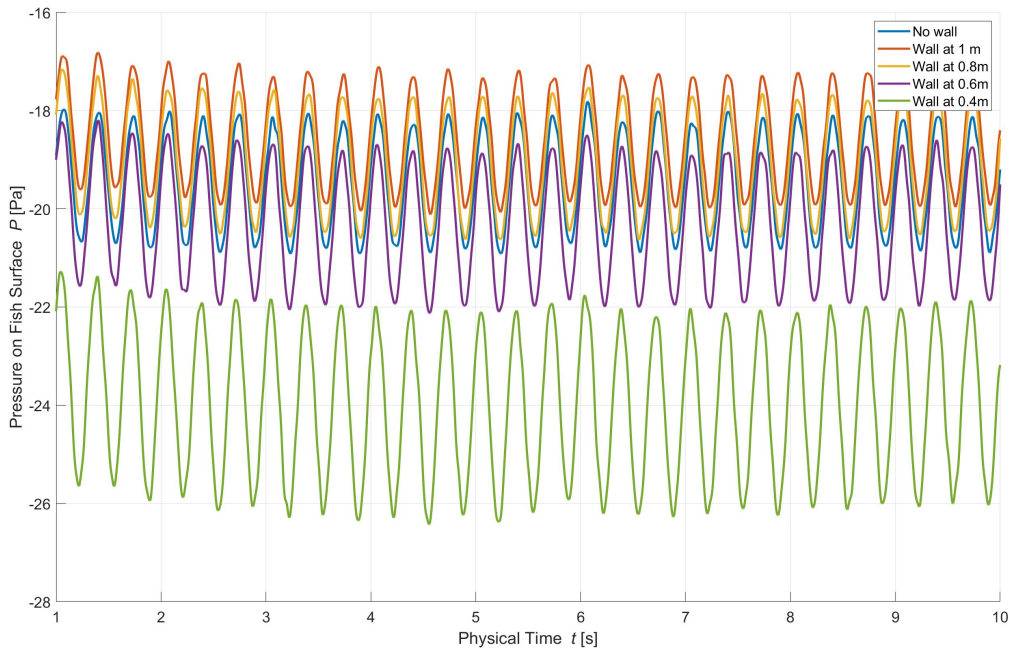
(b) Surface pressure average on the fish.

Figure 5.8: The simulation is first done with no walls on the sides, followed by two walls at different distances on the sides of the fish. The simulations are over a period of 10 s. The wall distances indicates the distance between the fish and the wall at each side, *i.e. h* is 2 times this distance.

5.3.3 One vs. Three fish

Figure 5.9 shows the vorticity field in z-direction for three fish. They where simulated in a system with walls on the sides 1 m away from the centre, *i.e.* $h = 2$ m. Figure 5.10 shows a comparison of the flow pressure average at the inlet plane for one fish vs. three fish in the system. Figure 5.11 (a) looks at the surface pressure average on each of the three fish compared to the one fish. Figure 5.11 (b)-(c) does the same for total forces in x-direction.
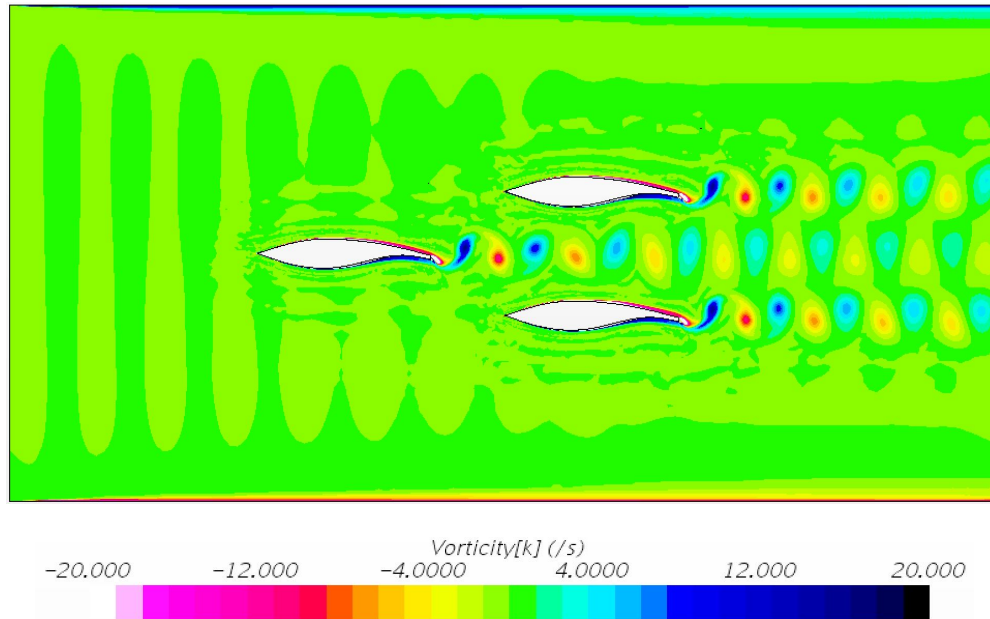

Figure 5.9: Vorticity field in z-direction for simulation of three 2-D fish in a system between two walls with $h = 2$ m.
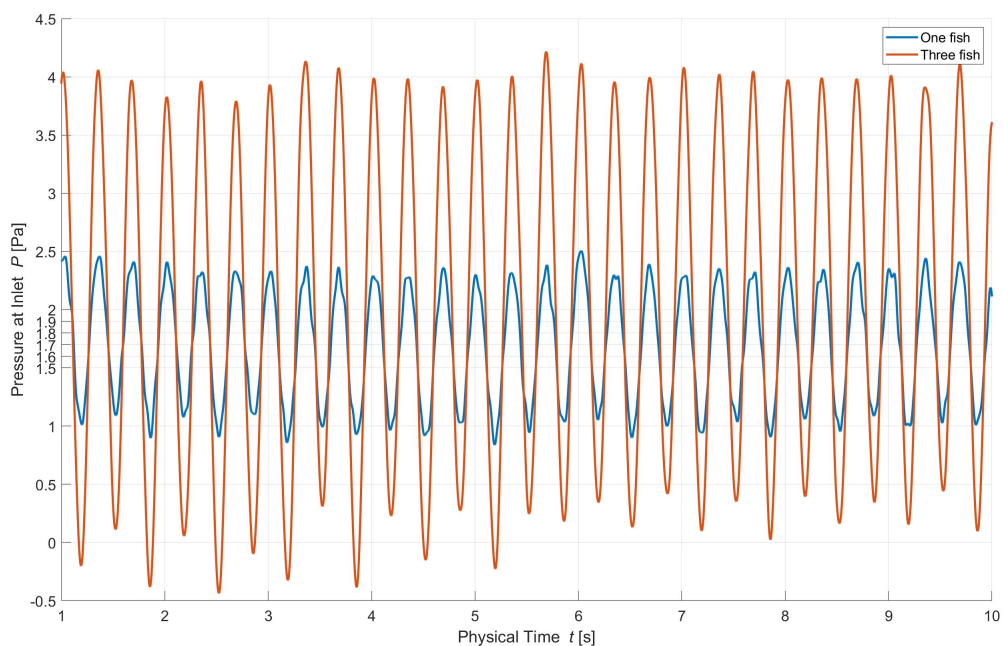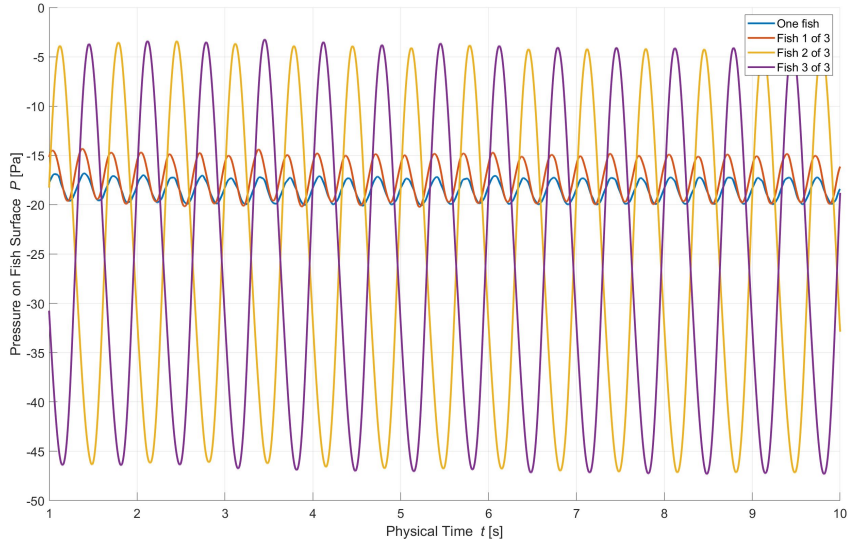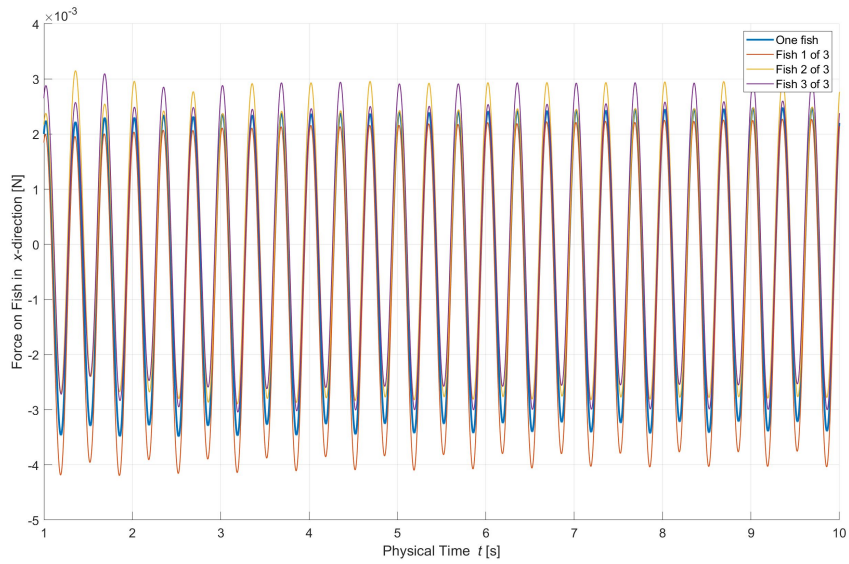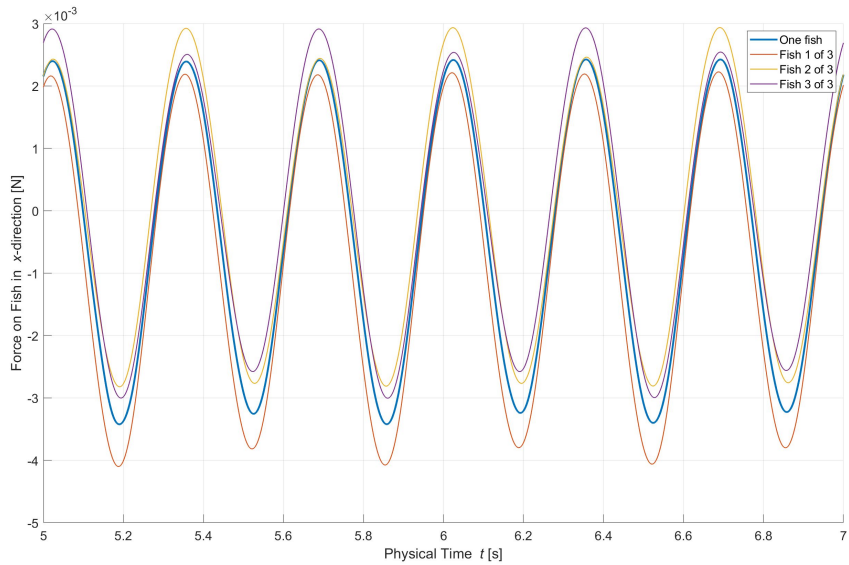

Figure 5.10: Comparing the flow pressure average at the inlet plane for a system with one vs. a system with three fish. The walls are 1 m from the centre, *i.e.* $h = 2$ m.

(a) Surface pressure average.

(b) Surface total x-force.

(c) Surface total x-force zoomed.

Figure 5.11: Comparing the sole fish with each of the three fish in a system with $h = 2$ m.

6. Discussion

This chapter will focus on discussing the results. The aim will be to link the findings to the literature, to theory, and to practice. An error analysis looking at the accuracy of the results will follow.

6.1   Boundary Layers

The boundary layer was simulated over a fixed smooth flat plate in parallel incoming flow. This section will discuss the Reynolds number used, the results obtained during the laminar simulation, and also the choice of a turbulence model suited for the simulation of fish.

6.1.1   Reynold's number

The Reynolds number was calculated to be $3.1 \cdot 10^5$ (Table 4.4) for a flow velocity of $U = 0.4$ m/s and fish length $L = 0.7$ m. Re_{crit} was said to be $5 \cdot 10^5$ for a boundary layer for flow over a parallel flat smooth plate in Section 2.2.5. This Re therefore gives a *laminar* boundary layer. For an adult carangiform swimmer however, the same Reynolds number gives a turbulent boundary layer, as discussed in Section 2.1.1. The velocity was therefore increased to 1.5 m/s to also simulate a fully *turbulent* boundary layer over flat plate.

6.1.2   Laminar Simulation

In Figure 5.2 (a) it is observed that the simulation with pointed end is closer to Blasius' analytical solution than the simulation with a flat end. This indicates that the closer one gets to a perfectly flat plate without any thickness to disturb the flow, the closer one gets to the analytical solution. A bigger deviation is observed at the front end of the plate than at the back end. This is due to the disturbances and possible flow separation occurring when the flow hits the plate.

Some bumps are observed at the simulated curves. These are also due to the disturbances occurring when the flow hits the plate. These bumps did not occur for the simulation in the specialization project [1] when the plate was placed as in Figure 3.2. All in all, this plot shows a good correspondence between the simulated and analytical plot of the laminar boundary layer thickness.

For the skin friction coefficient in Figure 5.2 (b) it is again observed that the pointed end simulation has a better approximation to Blasius' solution. At the back end of the plate both simulations jump away from Blasius' solution. This is as expected because of the thickness of the plate causing the water to separate from the plate due to the low pressure behind the plate. This is supported by looking at the velocity vectors at the back end of the plate in Figure 6.1, showing some back flow. Looking away from this, the simulated laminar boundary layer skin friction coefficient shows great correspondence with Blasius' solution.
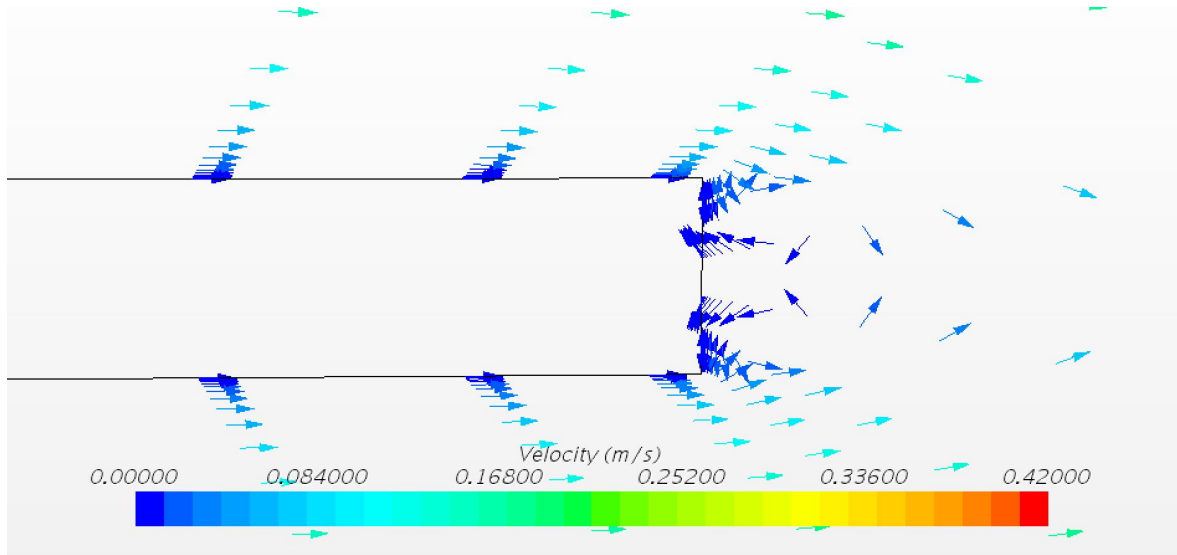
Figure 6.1: Back flow at the back end of the flat plate during simulation of its laminar boundary layer.

6.1.3 Choosing a Turbulence Model

The turbulent simulations did not show as good correspondence as the laminar simulation, but still good accuracy. In Figure 5.3 it is observed that both the boundary layer thicknesses and skin friction coefficients show lower values than the analytical solutions. This might be due to a relatively low Reynolds number of $1.2 \cdot 10^6$ or just the fact that the thickness of the plate disturbs the solutions quite allot. Another explanation might be that STAR-CCM+ turbulence models are tuned a bit low. The turbulence model was chosen on the basis of which one showed best correspondence *on average* with both the boundary layer thickness and the skin friction coefficient. Based on this, the standard k-ε two-layer was chosen as the most fitting turbulence model for modeling boundary layer effects over a flat smooth plate.

6.2 Carangiform Motion

The morphing tool was chosen for a thin plate with carangiform motion. How realistic the motion is according to the Strouhal number, how the motion turned out to be in STAR-CCM+, and the morphing grid deformation will be discussed in this section.

6.2.1 Strouhal Number

According to Eloy [37], 0.26 is the optimal Strouhal number for an Atlantic salmon of length 0.66 m, in $Re = 3.7 \cdot 10^5$. Our fish has a Strouhal number of 0.19 (Table 4.5). If the peak-to-peak tail tip had been only 0.02 m bigger, *i.e.* 1 cm in each direction, the Strouhal number would have been 0.26. This should also been expected as our fish is a bit longer than the fish considered in [37]. An optimal Strouhal number would optimize the thrust development, which should be an important factor when designing a closed fish farming system. If the aim is to have a system with constant flow speed, with fish standing against the current, it will be important not to exhaust the fish, and to let them swim as optimal as possible. The parameters in this thesis was however chosen to ensure zero force acting on the fish in x-direction, *i.e.* so that the fish is standing still in the incoming flow.

6.2.2 A Morphing System

Figure 5.4 shows a comparison of the carangiform position from STAR-CCM+ and analytical solutions at different time steps. The results are fitting the desired values. The simulated solution is only a bit off at some points, which can be explained by the fact that the approximation of the carangiform geometry (Figure 4.2) was using a spline only between 15 points, not the actual equation.

Figure 5.5 shows the grid deformation at the same time steps. It shows a nice grid without any overlapping of cells. It should be noted that the prism layer thickness seems to increase with time. If this is a bug in the STAR-CCM+ code or it is supposed to be like that is difficult to say. It does not a look like a good development as the cells close to the plate surface would probably be too big after a while, and the simulation would fail. This did not happen for the first 20 second of the simulation, so it didn't seem like a problem for investigating the fish further. The problem might have been fixed by using overset mesh instead of morphing mesh to only deform the cells closest to the thin plate.

6.3 The Atlantic Salmon

An approximation of the Atlantic salmon has been simulated in STAR-CCM+. This section will discuss the turbulent simulation compared to the laminar one, the surrounding flow, and a system with three fish compared to the same system with one fish.

6.3.1 Laminar vs. Turbulent

Even though it is already discussed that an adult fish with $Re = 3.1 \cdot 10^5$ has a turbulent boundary layer, it was decided to do a laminar and turbulent simulation of the fish with no walls to see if the results were any different. Figure 5.6 showed that all the values for the laminar solution are both lower and more unstable than the turbulent results. This is probably because the laminar simulation does not account for the turbulent effects. The difference is even more visible in Figure 5.7, where the area closest to the fish is nicely and smoothly shown for the turbulent simulation (b), but not for the laminar simulation (a). These results confirms that the turbulent viscous regime should be used when simulating a fish in this kind of Reynolds number.

6.3.2 The Surrounding Flow

In a closed fish farming system there are pumps pumping water at a given efficiency, and the flow velocity in the system can be measured before and after putting fish in it. This is a convenient and simple way to look at how the fish affect the flow, and is done in the experiments by Gorle *et al.* [27]. This can not be done in a control volume with constant velocity, and the effects therefore has to be measured in a different way.

As discussed in Section 2.2.2 fluid velocity is inversely proportional to fluid pressure. Increase in the fluid pressure as the walls on the sides of the fish comes closer is therefore the same as a decreased fluid velocity. This is clearly visible in Figure 5.8 (a). It starts at zero pressure when there are no walls on the sides, and when approaching only 0.4 m between the fish and the wall, the pressure has increased to around 5 Pa which is around 0.5 kg/m^2.

Figure 5.8 (b) plots the surface average pressure on the fish to see if the same is valid here. This was not the case, as the simulation with no walls ended up between walls at 0.8 m and 0.6 m from the fish. Looking away from the simulation with no walls, the pressure on the fish increased as the walls got closer in the other simulations. A possible explanation might be that the walls "release" some of the pressure from the fish up until a certain point where the walls got too close.

6.3.3 One vs. Three Fish

Three fish are placed according to the diamond shape discussed in Section 2.1.2. Figure 5.9 shows a reversed Kármán vortex street behind each fish. It was claimed that fish could save 10-20% energy by swimming in this positive flow, but this is not possible to account for in CFD.

The average fluid pressure at the inlet plane for the system with three fish is higher than for the same system with only one fish. This is shown in Figure 5.10, where the average value has increased from around 1.7 to 1.9 Pa. It is not a significant amount of pressure, only an increase of around 0.02 kg/m^2, but it is enough to believe that even more fish would increase the pressure further. For the surface pressure on the front fish it is observed in Figure 5.11 (a) that it has decreased a bit, but there is a bigger pressure on the two fish behind. The total force in x-direction in Figure 5.11 (b)-(c) lies around zero for all fish, which means that they are all standing still against the flow current.

6.4 Error Analysis

The results are all discussed based on the solutions received from STAR-CCM+. Due to the fact that an output is always given through CFD analysis, it is easy to naively trust in this output and draw the wrong conclusion. It is relatively easy to preprocess and run a simulation, but there are no warnings regarding the accuracy of the results, or if they are the results you are actually looking for. When looking at the error types presented in Section 2.2.6, only some of them are of interest in this thesis. Physical modeling and geometry approximation error, iterative convergence error and discretization error will be discussed.

6.4.1 Physical Approximation Error

The physical modeling error includes everything considered in Section 4.1.3 concerning the physics models. To minimize the physical modeling error the common fundamental problem concerning the boundary layer over flat plate was examined. As discussed above, these results corresponded very well to the literature both in the laminar and turbulent case. When moving on to morphing grid and fish geometry, these basic validations are difficult to implement. Assuming that the modelling error of these cases builds upon the modelling error of the flat plate problem, it is said that the physical modelling error is very small.

The geometry modeling error on the other hand gives big uncertainty to the results. Real fish are covered with mucus which makes the skin more slippery than a smooth wall. Fish also have details as fins, gills, mouth and eyes which are not accounted for. A fish's motion is not predictable, but is assumed here to be periodic and straight forward. A 2-D fish

does not account for the variation of the fish's height, where the thickness of its body and especially its tail varies a lot. An Atlantic salmon will not be alone in a closed system either, it will be surrounded by thousands of fish affecting one another. All these factors will affect the solution. However, assumptions and simplifications have been decisive to build generic fundamentals for the problem.

6.4.2 Iterative Convergence Error

The residuals for all runs are shown in Figure 6.2. They are shown for different wall distances for one fish (a)-(e), and for the simulation of three fish (f). The residuals are low and flat for all the runs, which indicates a steady-state solution with very small iterative convergence error. The reason why (f) has more color on the plot is that it was simulated for a smaller time step to keep the Courant number below one, *i.e.* more iterations during the 10 seconds.
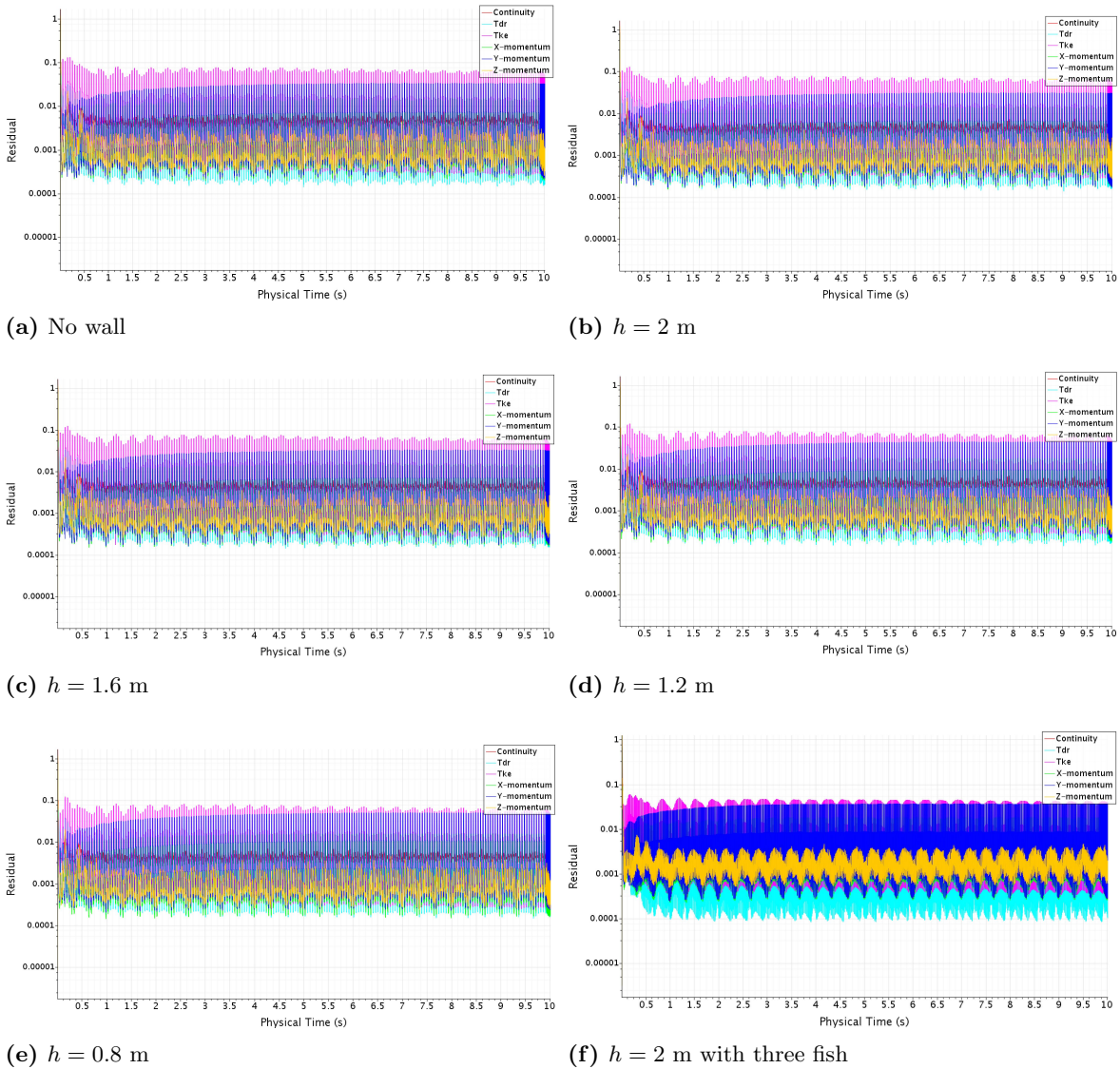

(a) No wall

(b) $h = 2$ m

(c) $h = 1.6$ m

(d) $h = 1.2$ m

(e) $h = 0.8$ m

(f) $h = 2$ m with three fish

Figure 6.2: Residuals for simulations of different wall distances for one fish (a)-(e), and for one simulation of three fish (f).

6.4.3 Spatial Discretization Error

The simulation with one fish without any walls are compared for three different grid refinements; base size 0.1 m, 0.08 m and 0.06 m. The comparison is shown in Figure 6.3. The fluid pressure at the inlet plane is compared to each other. All simulations appear to be giving the same result, which is what we strive to achieve. The y^+ was also made sure to be < 1 for all the turbulent simulations of fish. Examples of this are shown in Figure 6.4. It is quite difficult to see, but they are in the range or $0 < y+ < 1$, except for a small area on the tail of (a). This varies with the simulation and is not of any concern.
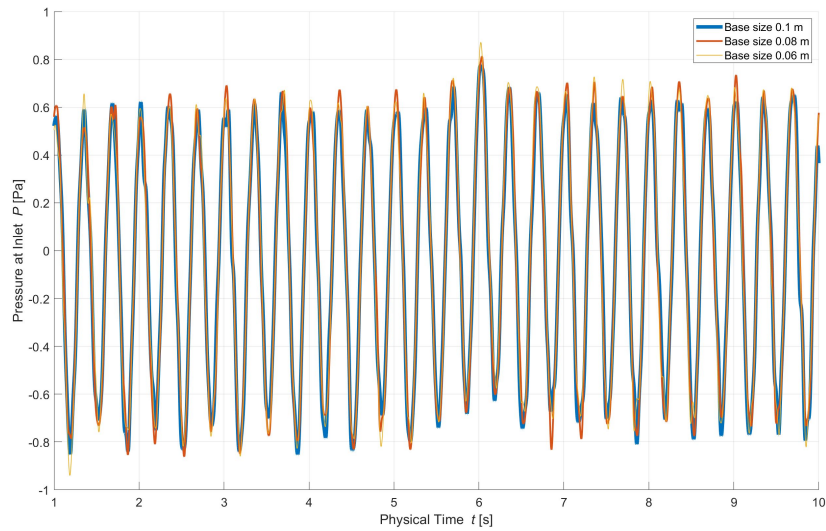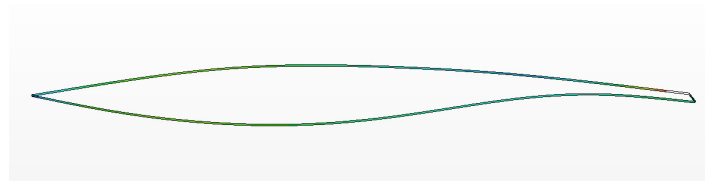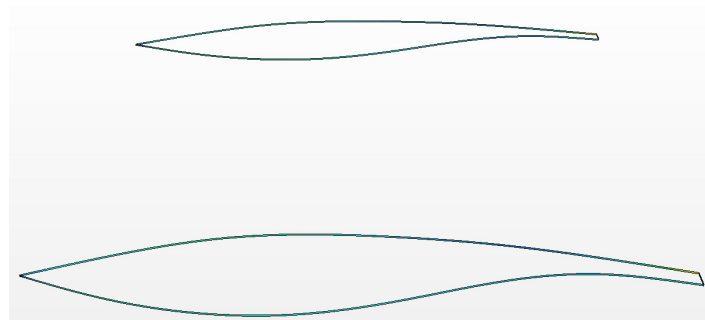

Figure 6.3: Comparing the grid refinement for three different base sizes of the simulation of one fish without any walls on the sides.
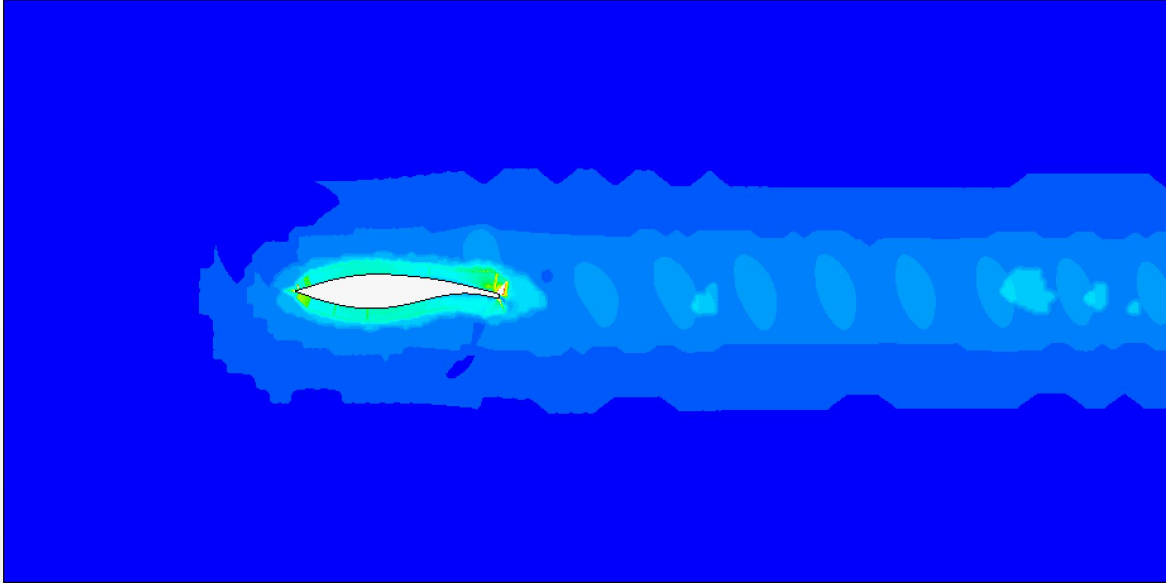

(a) Simulation of one fish.
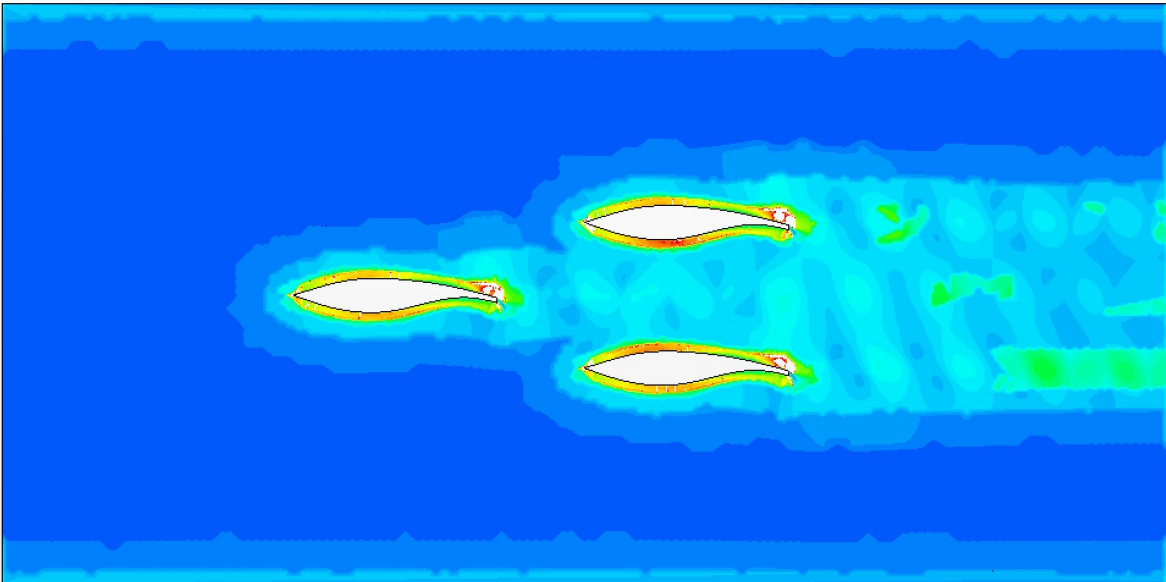

(b) Two fish from simulation of three fish.

Figure 6.4: y^+-value for two different simulations.

56

6.4.4 Temporal Discretization Error

A time step comparison was not conducted in this study as the simulations where run locally and would take too much time to run for very small time steps. It is also an implicitly unsteady time discretization, which means that the simulation always will be steady. The Courant number was however tested and required to be smaller than or equal to one to ensure the required accuracy in the turbulence calculations. Some examples of the Courant number are shown in Figure 6.5. It is visible in this figure as well that a small area close to the fish tail is exceeding 1.

(a) Simulation of one fish.

(b) Simulation of three fish.

Figure 6.5: Courant number for two different simulations.

7.   Conclusion and Continuation

CFD has been frequently used to do flow calculations inside closed fish farming cages. These calculations are done by neglecting the biomass and thereby the motion and possible effects fish might have on the flow conditions. Whether fish in closed fish farming cages will reduce, increase or do nothing to the flow velocity of the surrounding water has therefore been a topic of discussion in the industry. The objectives of this thesis have been to conduct CFD simulations of fish and their surrounding flow, to identify what the effects from fish in closed fish farming cages are and if they can be neglected, and to compare the results of the study to results found in literature.

7.1   Conclusions

A CFD study on how fish affect the flow inside closed fish farming cages have been conducted. A stepwise approach was followed in order to be able to validate one step before moving on to the next. The first step was to do a laminar and turbulent analysis of the boundary layer over a flat smooth plate in parallel flow. The standard k-ε turbulence model was chosen as the best model for calculating effects close to the boundary. This is important when doing CFD on fish, as its motion and following vortex street is dependent on the flow separation from its body. The second step was to implement a carangiform motion to a thin plate, and to test the grid deformation. The final step was to give the thin plate with carangiform motion a carangiform fish shape to simulate an Atlantic salmon. This case was simulated without and with walls on the sides of the fish at different distances to look at how fish affect the flow in a closed system. Based on the error analysis conducted in Section 6.4 it is concluded that the results obtained are validated with good accuracy and reliability. Simplifications of the geometry are the main source of possible deviation from a more realistic solution, and more detailed discretization error analysis should have been done.

Based on the results discussed in Section 6.3, fish are affecting the flow by increasing the pressure for smaller and smaller distance between the walls on the sides of the fish. This implies that fish would reduce the velocity in a closed system of constant fluid pressure. This is supported by the (only) article doing an experimental research on this. Whether the effects from fish on the surrounding flow is negligible when doing flow calculations in closed fish farming cages is difficult to say at this point as more investigation is needed. When doing a quick run of three fish in the system, it was concluded that more fish seems to have bigger effect on the surrounding flow. This indicates that investigation should be done on more fish before any crucial decisions are made.

7.2   Recommendations

Firstly, I would highly recommend to continue using MATLAB (or other simular software) as a supportive tool to STAR-CCM+. It is not possible to combine plots from different simulation files in STAR-CCM+, which is easily done by reading the exported .cvs files in MATLAB and plotting them in the same figures there.

When it comes to something I would have done differently, I would recommend to read more about what is expected in a CFD analysis, and especially the error analysis. I did not do this in advance, which gave me a lot of unexpected runs at the end of the research period regarding the grid refinement analysis, and did not get time to do any time step comparison simulations. Also, I would recommend trying to figure out how to do a design study of this problem in STAR-CCM+. It is not easy when the start position of the midline motion, and thereby the geometry, is dependent of the amplitude, in which is dependent on the tail beat frequency. Therefore, all simulations had to be done in individual simulation files, which is from my understanding, unnecessarily complicated.

I would recommend to run locally to be able to look at the simulations while they are running. However, if it is possible, use a workstation that is locally connected to a supercomputer to save hours of computational time. I would also recommend trying the overset mesh for grid deformation to see if this saves computational time, and if it is possible to avoid the increasing size of the grid cells close to the plate compared to the morphing tool.

Finally, I would recommend getting in touch with some of the interested companies from the survey study done in the specialization project. By doing this it would be possible to do simulations of the exact systems they use, with the correct size of fish and everything.

7.3   Further work

A more thorough discretization error analysis considering more grid refinements and time step refinement will be crucial to be able to say for sure that the results are reliable.

Then, more realistic cases would be of interest. More fish in the system, 3-D effects and details on the fish would possibly impact the results. When the simulations are as realistic as desired, it would make more sense to look at the results in terms of numbers, like how many percent fish reduce the flow velocity as a function of how high the density of fish is and in what kind of system.

Bibliography

[1] **Olsen H.** *Approaching a CFD Study on the Impacts Fish have on Surrounding Flow.* Tech. rep. Trondheim: Norwegian University of Science and Technology, Dec. 2018.

[2] **The Climate Group**. *Climate Week NYC Kicks off with Secretary John Kerry, Ban Ki-Moon and Apple Ceo Tim Cook, Ahead of UN Climate Summit.* `https://www.theclimategroup.org/what-we-do/news-and-blogs/climate-week-nyc-kicks-off-with-secretary-john-kerry-ban-ki-moon-and-apple-ceo-tim-cook-ahead-of-un-climate-summit/`. [News article; accessed May 7, 2019]. 2014.

[3] **United Nations**. *Report of the World Commission on Environment and Development: Our Common Future.* Tech. rep. New York, US: General Assembly, Aug. 1987.

[4] **United Nations**. *Resolution adopted by the General Assembly on 25 September 2015.* Tech. rep. New York, US: General Assembly, Oct. 2015.

[5] **United Nations**. *World Population Prospects: The 2017 Revision, Key Findings and Advance Tables.* Tech. rep. New York, US: Department of Economic and Social Affairs, June 2017.

[6] **FAO**. *The State of World Fisheries and Aquaculture 2018 – Meeting the sustainable development goals.* Tech. rep. Rome, Italy: Food and Agriculture Organization of the United Nations, 2018.

[7] **Tidwell J. H.** *Aquaculture Production Systems.* Wiley-Blackwell, 2012.

[8] **Masser M.P.** "What is Cage Culture?" In: *The Southern Region Aquaculture Center,* Vol. 160 (2008).

[9] **PwC**. *Sustainable growth towards 2050 – PwC Seafood Barometer 2017.* Tech. rep. Bergen: Pricewaterhouse Coopers International Limited, Nov. 2017.

[10] **Norwegian Directorate of Fisheries**. *Development Licenses.* `https://www.fiskeridir.no/Akvakultur/Tildeling-og-tillatelser/Saertillatelser/Utviklingstillatelser`. [Information site; accessed May 7, 2019]. 2018.

[11] **Liu H; Wassersug R. J; Kawachi K. A;** "A Computational fluid dynamic study of tadpole swimming". In: *The Journal of Experimental Biology,* Vol. 199.6 (1996), pp. 1245–60.

[12] **Lyttle A. D; Blanksby B. A; Elliot B. C; Lloyd D. G;** "Net forces during tethered simulation of underwater streamlined gliding and kicking techniques of the freestyle turn". In: *Journal of Sports Science,* Vol. 18.10 (2000), pp. 801–807.

[13] **Takagi T; Tamura Y; Weihs D;** "Hydrodynamics and energy-saving swimming techniques on Pacific bluefin tuna". In: *Journal of theoretical biology,* Vol. 336 (2013), pp. 158–172.

[14] **Liang Y.** and **Yu-min S.** "CFD Simulation of Flow Features and Vorticity Structures in Tuna-Like Swimming". In: *China Ocean Engineering Society,* Vol. 25.1 (2011), pp. 73–82.

[15] **Li N; Liu H; Su Y;** "Numerical study on the hydrodynamics of thunniform bio-inspired swimming under self-propulsion". In: *Public Library of Science ONE,* Vol. 12.3 (2017), pp. 1–36.

[16] **Kern S.** and **Koumoutsakos P.** "Simulations of optimized anguilliform swimming". In: *The Journal of experimental biology,* Vol. 209.24 (2006), pp. 4841–57.

[17] **Borazjani I.** and **Sotiropoulos F.** "Numerical investigation of the hydrodynamics of carangiform swimming in the transitional and inertial flow regimes". In: *The Journal of experimental biology,* Vol. 212.4 (2008), pp. 576–592.

[18] **Borazjani I.** and **Sotiropoulos F.** "On the role of form and kinematics on the hydrodynamics of self-propelled body/caudal fin swimming". In: *The Journal of experimental biology,* Vol. 213.1 (2010), pp. 89–107.

[19] **Li G; Müller U. K; van Leeuven J. Liu H;** "Body dynamics and hydrodynamics of swimming fish larvae: a computational study". In: *The Journal of experimental biology,* Vol. 215.22 (2012), pp. 4015–33.

[20] **Cui Z; Gu X; Li K; Jiang H;** "CFD Studies of the Effects of Waveform on Swimming Performance of Carangiform Fish". In: *Applied science,* Vol. 7.2 (2017), pp. 1–17.

[21] **Hannon J. W.** *Image based computational fluid dynamics modeling to simulate fluid flow around a moving fish.* Tech. rep. Iowa, US: University of Iowa, July 2011.

[22] **Adkins D.** and **Yan Y.** "CFD simulation of fish-like body moving in viscous liquid". In: *Journal of Bionic Engineering,* Vol. 3.3 (2006), pp. 147–53.

[23] **Reid D. A. P; Hildenbrandt H; Padding J. T; Hemelrijk C. K;** "Fluid dynamics of moving fish in a two-dimensional multiparticle collision dynamics model". In: *Physical review,* Vol. 85.2 (2012), pp. 1–15.

[24] **Lee J. E; Hoon C. P; Choi H. S; Kyung J; Yun D; Jeong S; Ryu Y;** "Numerical Simulation of Biomimetic Robot Fish". In: *International Conference on Control, Automation and Systems,* Vol. 13 (2013), pp. 890–93.

[25] **Zouh H; Hu T; Low K; Shen L; Ma Z; Wang G; Xu H;** "Bio-inspired Flow Sensing and Prediction for Fish-like Undulating Locomotion: A CFFD-aided Approach". In: *China Ocean Engineering Society,* Vol. 25.3 (2015), pp. 406–417.

[26] **Johansson D; Laursen F; Fernö A; Fosseidengen J; Klebert P; Stien L; Vågseth T; Oppedal F;** "The Interaction between Water Currents and Salmon Swimming Behaviour in Sea Cages". In: *Public Library of Science ONE,* Vol. 9.5 (2014), pp. 1–4.

[27] **Gorle J. M. R; Terjesen B. F; Mota V. C; Summerfelt S;** "Water velocity in commercial RAS culture tanks for Atlantic salmon smolt production". In: *Aquacultural Engineering,* Vol. 81.C (2018), pp. 89–100.

[28] **Sfakiotakis M; Lane D. M; Davies J. B;** "Review of Fish Swimming Modes for Aquatic Locomotion". In: *Institute of Electrical and Electronics Engineers journal of oceanic engineering,* Vol. 24.2 (1999), pp. 237–252.

[29] **Lindsey C. C.** "Form, function and locomotory habits in fish". In: *Fish Physiology,* Vol. 7 (1978), pp. 1–100.

[30] **Videler J. J.** *Fish Swimming.* Chapman and Hall: London, 1993.

[31] **Alvarado P. V. Y.** *Design of biomimetic compliant devices for locomotion in liquid environments.* Tech. rep. Massachusetts: Massachusetts Institute of Technology, Departments of Mechanical Engineering, Jan. 2007.

[32] **Anderson E. J; McGillis W. R; Grosenbaugh M. A.** "The boundary layer of swimming fish". In: *Journal of Experimental Biology,* Vol. 204.1 (2001), pp. 81–102.

[33] **Webb P. W.** "Simple physical principles and vertebrate aquatic locomotion". In: *American Zoologi,* Vol. 28.2 (1988), pp. 709–25.

[34] **Lighthill M. J.** "Hydromechanics of aquatic animal propulsion". In: *Annual review of fluid mechanics,* Vol. 11.1 (1969), pp. 413–46.

[35] **Alexander R. M.** *Functional Design in Fishes.* Hutchinson University Library, 1967.

[36] **Triantafyllou G. S; Triantafyllou M. S; Grosenbauch M. A;** "Optimal thrust development in oscillating foils with application to fish propulsion". In: *Journal of fluids and structures,* Vol. 7.2 (1993), pp. 205–224.

[37] **Eloy C.** "Optimal Strouhal number for swimming animals". In: *Journal of fluids and structures,* Vol. 30.C (2012), pp. 205–18.

[38] **Weihs D.** and **Webb P. W.** *Optimization of locomotion.* New York: Praeger, 1983.

[39] **Pletcher R. H; Tannehill J. C; Anderson D. A;** *Computational Fluid Mechanics and Heat Transfer.* CRC Press Taylor & Francis Group, 2012.

[40] **Cengel Y. A.** and **Cimbala J. M.** *Fluid Mechanics; fundamentals and applications (third edition in SI units).* United States: McGraw-Hill Education, 2014.

[41] **Moukalled F; Mangani L.; Darwish M;** *The Finite Volume Method in Computational Fluid Dynamics.* Cham: Springer International Publishing, 2015.

[42] **Blazek J.** *Computational Fluid Dynamics: Principles and Applications (third edition).* United Kingdom: Butterworth-Heinemann, 2015.

[43] **Xiao H.** and **Cinnella P.** "Quantification of Model Uncertainty in RANS Simulations: A Review". In: *Progress in Aerospace Sciences,* (2018).

[44] **Alfonsi G.** "Reynolds-Averaged Navier-Stokes Equations for Turbulence Modeling". In: *Applied Mechanics Reviews,* 62.4 (2009), pp. 040802-1–20.

[45] **Mathew J.** "Large Eddy Simulation". In: *Defence Science Journal,* 60.6 (2010), pp. 598–605.

[46] **Blasius H.** "The boundary layers in fluid with little friction (Grenzschichten in flüssigkeiten mit kleiner reibung)". In: *Zeitschrift für Mathematik und Physik,* Vol. 56.1 (1908), pp. 1–37.

[47] **AAIA**. "Guide for the verification and validation of Computational Fluid Dynamics Simulations". In: *American Institute of Aeronautics and Astronautics,* G.077 (1998).

[48] **SIEMENS**. *STAR-CCM+.* `https://mdx.plm.automation.siemens.com/star-ccm-plus`. [Information page; accessed May 7, 2019]. 2018.

List of Figures

List of Tables

List of Symbols and Acronyms

Nomenclatures

A	wake width	[m]
a_i	quadratic coefficients of the amplitude envelope	[–]
b	computational domain width	[m]
C_D	drag coefficient	[–]
C_f	local skin friction coefficient	[–]
d	computational domain depth	[m]
f	tail beat frequency	$\frac{\omega}{2\pi}$ [Hz]
F_D	viscous drag force	[N]
H	distance between two fish in the same column	[m]
h	computational domain height	[m]
k	wave number	[–]
L	fish length	[m]
p	fluid pressure	[Pa]
Re	Reynolds number	$\frac{LU}{\nu}$ [–]
S	wetted surface area	[m^2]
St	Srouhal number	$\frac{fA}{U}$ [–]
t	time	[s]
U	characteristic velocity	[m/s]
u	local fluid velocity in x-direction	[m/s]
u_T	friction velocity	[m/s]
V	propagating speed	[m/s]
v	local fluid velocity in y-direction	[m/s]
x	horizontal coordinate	[m]
y	vertical coordinate	[m]
y^+	dimensionless distance to the wall	[–]

z	outward coordinate	[m]

$a(x)$	fish motion amplitude	
$R(x)$	half height of cross section	
$r(x)$	half width of cross section	
$y(x,t)$	mid line fish motion in vertical direction	

$\vec{F}$	vector sum of forces	[kgms^{-2}]=[N]
$\vec{g}$	gravitation acceleration	9.81 [m/s^2]
$\vec{p}$	rate of change of momentum	[kgms^{-1}]=[Ns]
$\vec{u}$	flow velocity vector field	[m/s]

Δt	time step	[s]
Δx	space step	[m]
δ	boundary layer thickness	[m]
η	change of variable y in boundary layer	[–]
μ	dynamic viscosity	$8.887 \cdot 10^{-4}$ [Pa·s]
μ_T	eddy-viscosity	[m^2/s]
∇	nabla operator	[–]
ν	kinematic viscosity	$\frac{\mu}{\rho}$[m^2/s]
ω	tail beat frequency	[s^{-1}]
ρ	density	997.56 [kg/m^3]

Abbreviations

2-D	two-dimensional
3-D	three-dimensional
AKN	Abe-Kondoh-Nagano
BCF	body and/or caudal fin
BvK	Bénard-von Kármán
CAD	computer-aided design

CFD	computational fluid dynamics
CFL	Courant-Friedrichs-Lewy
DNS	direct numerical simulation
EB	Elliptic Blending
FVM	finite volume method
HDPE	high density polyethyle
IMT	Department of Marine Technology
k-ϵ	k-epsilon turbulence model
k-ω	k-omega tubulence model
LES	large-eddy simulation
MPF	median and/or paired fin
NTNU	Norwegian University of Science and Technology
PDE	partial differential equation
R&D	research and development
RANS	Reynolds averaged Navier-Stokes
RAS	recycling aquaculture systems
rBvK	reversed Bénard-von Kármán
RS	Reynolds stress
S-A	Spalart-Allmaras
SDG	sustainable development goal
SST	Shear Stress Transport
UN	United Nations

Appendices

A   Project Description

NTNU
Norges teknisk-naturvitenskapelige universitet
Institutt for marin teknikk
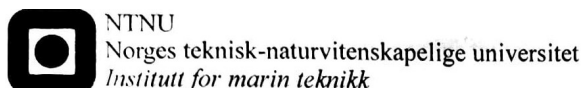
HOVEDOPPGAVE I MARIN HYDRODYNAMIKK

Vår 2019

FOR

Stud.techn. Hannelore Olsen

Simulering av strømning omkring fisk

Kandidaten skal sette seg inn i teori for numerisk beregnuing av strømning samt hydrodynamikk rundt fisk og fiskens bevegelsesmønster. Dataprogrammet STAR CCM+ kan brukes til å begerne strømning rundt fiske. Kandidaten skal sette seg inn i programmet og dets muligheter og begrensninger. Videre skal kandidaten modellere og beregnge størmining rundt forenklede modeller av en fisk. Ulike turbulens modeller skal utforskes.
Om tiden tillater det skal kandidaten regne full strømning rundt fisk i tre dimensjoner, eventuelt regne på flere fisker med en forenklet modell. Interaksjon mellom omgivelser og mellom ulike fisker er av interesse.

Det forutsettes at Institutt for marin teknikk, NTNU, fritt kan benytte resultatene i sitt forskningsarbeid, da med referanse til studentens arbeid.

Besvarelsen redigeres mest mulig som en forskningsrapport med resymé, konklusjon, litteraturliste etc. Ved utarbeidelsen av teksten skal kandidaten legge vekt på å gjøre den så kort, oversiktlig og velskrevet som mulig.

Besvarelsen leveres i to eksemplar innen 11. juni 2019.

Håvard Holm
1.amanuensis

B   Poster

A CFD Study on how Fish Affect the Flow Inside Closed Fish Farming Cages

Student Hannelore Olsen; Supevisor Håvard Holm; Co-supervisor Hans Jørgen Bjelke Mørch

Department of Marine Technology, Norwegian University of Science and Technology

Objectives

Whether fish in closed fish farming cages will reduce, increase or do nothing to the flow conditions and velocity of the surrounding water is a topic of discussion. How do fish affect the surrounding water? Is it okay to neglect the effects from fish when analyzing the flow in closed fish farming cages? How are the results compared to the literature? The objectives to answer these questions are

- to conduct CFD simulations of fish and its surrounding flow,
- to identify if the effects from fish in closed fish farming cages are negligible by analyzing the simulations, and
- to compare the results from this study to results found in literature.

Introduction

The term **sustainable** is about taking care of the needs humans have today, without compromising future generations. In a sustainable community there is balance between social, economical and environmental relationships. The 17 Sustainable Development Goals (SDGs) are created to help us achieve this balance.

An increasing world population creates the problem of providing food and livelihood to all in a sustainable way. The State of World Fisheries and Aquaculture 2018 [1] claims that agriculture is key to achieve this. The SDGs related to this is shown in the figure below. The current production platforms based on open systems are too weak to sustain significant growth, recognized environmental performance and societal expectations. Therefore, new aquaculture technology are being developed.

Closed fish farming cages are one of these new technologies. Detailed calculations are needed to control the environmental factors inside such a system. These are currently done without considering how the motion of fish will affect the flow conditions.

Figure: SDGs related to aquaculture.

CFD with STAR-CCM+

The central process in computational fluid dynamics (CFD) is discretization; taking fundamental equations (PDEs) with an infinite number of degrees of freedom and reducing them to a system of finite degrees of freedom. The PDEs are then reduced to a system of algebraic equations that can be solved on a computer.

STAR-CCM+ is an all-in-one multidisciplinary CFD software for the simulation of products and designs operating under real-world conditions. Ultimately, these results are of higher quality than hand calculations and experimental testing of physical prototypes, in a more cost efficient way.
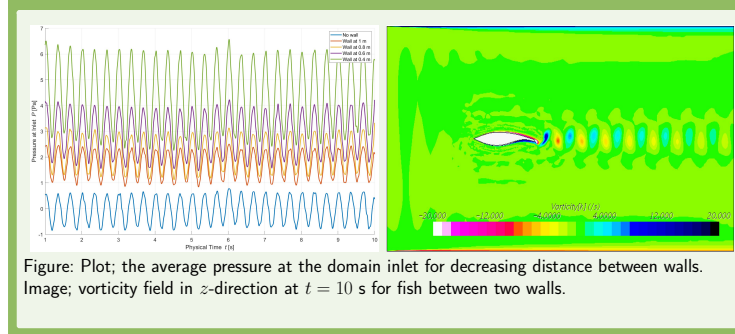
Important Result

Figure: Plot; the average pressure at the domain inlet for decreasing distance between walls. Image; vorticity field in z-direction at $t = 10$ s for fish between two walls.

Method

CFD simulations where each simulation builds on the validity and reliability of the previous one was conducted. Their domain sketches are shown in the figure below, and are called

1. fixed flat plate,
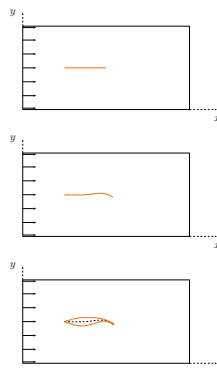2. plate with carangiform motion,
3. 2D carangiform fish.

Figure: Domain sketches of the procedure.

Fish Shape and Motion

The parameterized kinematics law of body and/or caudal fin (BCF) motions is described as

$$y(x,t) = a(x)\sin(kx - \omega t),$$

with $y(x,t)$ the mid line motion at point x and time t, ω the tail-beat frequency, and k the wave number. The function $a(x)$ is defined for carangiform motion [2] as $a(x) = a_1 + a_2 x + a_3 x^2$ where the constants a_1, a_2 and a_3 are quadratic coefficients of the amplitude envelope.

The cross-section of carangiform fish can be defined as an ellipse with half-width $r(x)$ as [3]

$$r(x) = 0.045L\sin\left(\tfrac{2\pi}{1.25L}x\right) + 0.06L\left(e^{\frac{2\pi}{3.14L}x} - 1\right).$$

Results

The standard k-ε two-layer turbulence model proved to be best to simulate the boundary layer over flat plate, and was therefore used through the rest of the simulations.

The plot in the figure above presents the average pressure value at the domain inlet. With no wall on the sides of the fish, the pressure is zero. When adding walls (and further decreasing the distance between them) the pressure at the inlet increases from 0 to 5 Pa, or 5 Newton per square meter, which is about 0.5 kg/m². It is supported by experiments that the velocity will be reduced in such a system [4].

The image to the right of the plot is a screenshot from STAR-CCM+ showing the vorticity distribution in z at time step $t = 10$ s. Red is clock-wise and blue is counter clock-wise, which shows a reversed Kármán street behind the fish.

Conclusion

The fluid pressure increased at the inlet face when the distance between the walls where decreased. This implies that the fluid velocity would be reduced in a closed fish farming system with constant pressure, as fluid velocity is inversely proportional to fluid pressure. It is supported by literature that the velocity will be reduced when adding fish to such a system. Finally, it is difficult to say if the effects caused by fish are negligible when doing flow calculations in closed fish farming cages until further investigation has been done with more realistic case as e.g. several 3-D fish.

References

[1] **FAO**.
The state of world fisheries and aquaculture 2018 – meeting the sustainable development goals.
Technical report, Rome, Italy, 2018.

[2] **Videler J. J.**
Fish Swimming.
Chapman and Hall: London, 1993.

[3] **Alvarado P. V. Y.**
Design of biomimetic compliant devices for locomotion in liquid environments.
Technical report, Massachusetts, 2007.

[4] **Gorle J. M. R; Terjesen B. F; Mota V. C; Summerfelt S;**.
Water velocity in commercial ras culture tanks for atlantic salmon smolt production.
Aquacultural Engineering, 81(C):89–100, 2018.

Acknowledgements

NTNU   CFD marine

Håvard Holm   Hans J. B. Mørch

Contact Information

Hannelore Olsen

- https://www.linkedin.com/in/hanneloreolsen/
- hanneloo@stud.ntnu.no

C Turbulence Models Description

Turbulence model	Description
Abe-Kondoh-Nagano (AKN) Low-Re	Has different damping coefficients than the Standard K-Epsilon model, and uses different damping functions than the Standard Low-Re model. It is a good choice for applications where the Reynolds numbers are low but the flow is relatively complex.
Elliptic Blending (EB)	An adaptation and development of the elliptic relaxation model to two-equation type eddy viscosity model. The benefits of this model are that it has much improved performance in the near wall region and improved stability over the orginal K-Omega SST model.
Lag EB	Combines the standard EB model with the stress-strain lag concept. In most 3 dimensional turbulent flows, there will exist non-equilibrium effects that result in a misalignment of the principal components of stress and strain on the fluid. In situations like these, traditional RANS models tend to over predict the turbulent kinetic energy because they inherently are unable to account for such lag effects between stress and strain in fluids. The Lag EB model accounts for this misalignment and has further improvements over traditional RANS models in modeling the effects of anisotropy, curvature, and rotational flows. As a result, it is a very attractive option for a variety of applications.
Realizable	Differs from the Standard K-Epsilon model in that it contains a new formulation for the turbulent viscosity and it has a new transport equation for the dissipation rate ε which is derived from an exact equation for the transport of the mean-square vorticity fluctuation. The term realizable means that the model satisfies certain mathematical constraints on the Reynolds stresses.
Realizable Two-Layer*	Combines the Realizable model with the two-layer approach. The coefficients in the model are identical, but the model gains the added flexibility of an all $y+$ wall treatment.
Standard	This is the standard version of the two-equation model that involves transport equations for the turbulent kinetic energy k and its dissipation rate ε.
Standard Low-Re	This model has identical coefficients to the Standard model, but provides more damping functions. These functions let it be applied in the viscous-affected regions near walls.

Standard Two-Layer	Combines the Standard model with the two-layer approach, which allows the model to be applied in the sublayer. In the layer next to the wall, the turbulent dissipation rate ε and the turbulent viscosity μ, are specified as functions of wall distance. The values of ε specified in the near-wall layer are blended smoothly with the values computed from solving the transport equation far from the wall.
V2F	Known to capture the near-wall turbulence effects more accurately. It is based on the root mean square normal velocity fluctuations as the velocity scale rather than turbulence kinetic energy, thus it is capable of handling the wall region without the need for the additional damping functions because the normal velocity fluctuations are known to be quite sensitive to the presence of wall and thus are like a natural damper. The model employs four transport equations for the closure of the RANS equations, solving two more turbulence quantities, namely the normal stress function and the elliptic function, in addition to k and ε.
Shear Stress Transport (SST) Menter*	Takes advantage of accurate formulation of the k-ω model in the near-wall region with the free-stream independence of the k-ε model in the far field. It does so multiplying the final additional term, obtained from deriving the k-ε model, by a blending function. Close to wall the damped cross-diffusion derivative term is zero (leading to the standard ω equation), whereas remote from wall the blending function is unity (corresponding to the standard ε equation).
Standard (Wilcox)	Has seen most application in the aerospace industry. Therefore, it is recommended as an alternative to the Spalar-Allmaras models for similar types of applications.